



Università di Pisa

Facoltà di Scienze Matematiche, Fisiche e Naturali

Corso di Laurea Magistrale in Fisica

Anno Accademico 2014-2015

TESI DI LAUREA MAGISTRALE

**Experimental investigations of many-body
and multi-level effects in cold Rydberg gases**

CANDIDATO

Deborah Capecchi

RELATORE

Dr. Oliver Morsch

Introduction

Many-body physics studies systems composed of a large number of basic constituents, in which the scaling of the systems leads to the emergence of new and surprising properties [1]. Although the fundamental laws governing the physics of the constituents lie at the root of the many-body behavior, prediction of the emergent properties from the laws of the constituents and their correlations represents a thorny problem. On the one hand the correlations created by the interactions prevent a direct analytical approach to the problem, unless severe simplifications and approximations are applied. On the other hand the high number of degrees of freedom requires huge computational resources that are close to the limit of current technological capabilities and, in the case of quantum many-body systems, exceed them [2].

An experimental approach to the problem can open a third interesting way to predict many body effects.

The idea is to imitate or “simulate” the system we want to study with another many-body system, that has well controllable properties of its constituents and is easier to observe. Then, if we are able to produce such a system, we can observe directly how the manipulation of the properties of the constituents modifies the many-body behavior. The beauty of this approach lies in the fact that it does not require any predictive model nor does it impose any hypothesis on the emergence, but just “*let nature do it*” [3].

Cold Rydberg gases are well suited to this approach [4] as they have strong, long range tunable interactions and can easily be detected. In order to be able to perform a mapping of the original system onto a model system composed of Rydberg atoms – typically an Ising-type model of interacting spin 1/2 particles – we need a simple representation that helps to separate single-particle dynamics from manybody behavior. In the case of Rydberg atoms such a representation is usually given in terms of a two-level model

considering only the ground and the excited states. However not only manybody effects, which we are mainly interested in, modify the two level picture by shifting the energy of the excited state, but also the multi-level atomic structure modifies the model with the introduction of additional levels.

In this thesis we report the experimental investigation of many-body and multi-level effects in cold Rydberg atoms. The aim of this thesis is to identify the range of validity of the two-level approximation and its limitations, and to develop a technique that allows us to clearly identify many-body and multi-level effects.

The thesis starts by recalling in Chapter 1 the properties of Rydberg atoms, focusing on the van der Waals interactions that are responsible for many-body effects in our system. The experimental apparatus is then described in Chapter 2 introducing the main techniques we use for the trapping of the ground state atoms, the excitation of atoms from the ground state to the Rydberg state and the detection of Rydberg atoms. Trapping and excitation will be taken up again in Chapter 3 to introduce multi-level effects in low excited states. There we will discuss limitations of the trapping scheme itself and how to overcome them by using additional lasers, as well as the emergence of additional excitation pathways to the Rydberg state that complicate the simple two-level picture. The remainder of Chapter 3 is dedicated to the peculiar multi-level behavior of Rydberg gases, whereby the black-body radiation of a room temperature environment can couple the originally excited Rydberg state to other nearby Rydberg states. Due to this effect, over time, the content of the original Rydberg state populated during excitation can be spread over a number of different Rydberg states, each with its own properties.

Both many-body and multi-level effects on Rydberg state are probed with a de-excitation technique. That technique couples atoms with a specific energy to a fast decaying state from which they decay spontaneously to the ground state. In this way the atoms coupled by de-excitation are effectively removed from the detected sample. The cornerstone of this technique lies in the term “fast” defining the intermediate state. Ideally, “fast” means that the state is empty at all times during de-excitation. In a real experiment this is necessarily an approximation so that the definition of “fast” is that the level has negligible population at all times. The definition of the limits within which we can consider the intermediate state “fast” and the expedients to improve this approximation are described in detail in Chapter 4. The characterization of the de-excitation technique used in this thesis, contained in Chapter 4, creates the basis for its application in

the investigation of many-body effects reported in Chapter 5 and in that of multi-level effects reported in Chapter 6.

Chapter 5 and Chapter 6 do not have a hierarchical order of reading, however the results therein on many-body and multi-level effects are strongly connected as there is no way to prevent one or the other effect in Rydberg gases. Neglecting one or the other effect is just an approximation possible only within a narrow set of parameters. Definition of the working condition of each chapter, therefore, are cross-referenced to the other.

In the investigation of many-body effects reported in Chapter 5, the de-excitation technique introduces a simpler dynamics that allows us to extract complementary information with respect to experiments in which the excitation dynamics is studied. We are able to show that the excited state is either broadened, shifted or split by the van der Waals interactions between Rydberg atoms. We demonstrate that such deformations of the excitation spectrum hold information on the spatial configuration of strongly interacting Rydberg clusters and on the cross-over between the interacting and non-interacting regime.

In the study of multi-level effects de-excitation allows one to separate the population of the original Rydberg state from that of the other Rydberg states, populated by the black body radiation-induced transfers or other potential effects. This separation allows us to deduce on which timescale multi-level effects play a relevant role. Consequently we can evaluate on which timescale the two-level model, modified to account for many-body behavior, can be used to represent Rydberg atoms. De-excitation allows us also to measure the lifetime of the original Rydberg state in the light of all potential decay channels.

The results of this thesis describes the limits of the two-level models in our experiment.

My contribution to the work presented in this thesis consists in:

- the experimental characterization of the de-excitation technique as a tool to probe many-body and multi-level effects
- the experiment on the many-body effects in different interacting regimes
- the experiments on multi-level effects in Rydberg atoms due to the intermediate state used in the excitation protocol and due to the proximity of other Rydberg levels

During the thesis I was hosted for two months in the 5 Physikalisches Institut of Stuttgart university under the supervision of Dr. Robert Löw, where I contributed

to the set-up of a repump laser for Rb. Some of the technical results obtained during my stay in Stuttgart are reported in Appendix A.

Furthermore the results presented in Chapter 5 are part of a publication currently in preparation.

Contents

Introduction	iii
1 Properties of Rydberg atoms	1
1.1 General properties	1
1.2 van der Waals interactions and dipole blockade	2
1.3 Coherent and Incoherent regimes	6
1.4 Resonant and off-resonant excitation dynamics	7
2 Experimental apparatus	11
2.1 Overview	11
2.2 Magneto Optical Trap	11
2.3 Excitation	15
2.4 Detection	18
3 Multi-level effects	21
3.1 Multi-level in low lying states	21
3.2 Multi-level effects in Rydberg states	23
3.2.1 6p hyperfine structure	23
3.2.2 State transfer from black body radiation	24
4 De-excitation	29
4.1 Introduction and experimental protocol	29
4.2 Population of $6P_{3/2}$ and darktime	32
4.3 Coherent dynamics, Rabi frequency and slowdown of de-excitation	34
4.4 Conclusion	36
5 De-excitation as a probe of many-body effects	39
5.1 A simpler dynamics	39

5.2	On resonance excitation	40
5.3	Off-resonant excitation	45
5.4	Conclusion	47
6	De-excitation as probe of multi-level effects	51
6.1	Long dynamics and MOT decay	51
6.2	70s and support lifetime	54
6.3	Beyond 70S lifetime	57
6.4	Conclusion	61
	Conclusion	63
A	An example of repump laser	65

Chapter 1

Properties of Rydberg atoms

1.1 General properties

Rydberg atoms are atoms in highly excited energy levels with large principle quantum number $n > 20$, which have enhanced properties with respect to the ground state atoms. Among the most remarkable properties of Rydberg atoms are the high polarizabilities that enable strong long range interactions, which in a sufficiently dense sample of such atoms, give rise to many-body effects. Another feature that is relevant for the purposes of this thesis are the very long lifetimes ranging from 50 to 200 μs , that allow us to observe the action of manybody effects in the experiments. These properties make Rydberg atoms highly suitable candidates to simulate many-body physics.

The properties of Rydberg atoms can be derived in a hydrogen-like description that takes inspiration from the Rydberg spectral lines of hydrogen. The description dates back to the work of Johannes Rydberg (from which Rydberg atoms take their name), who extended the Balmer model for the spectral line of hydrogen to all excited states, obtaining the law for the energies E_n of those states:

$$E_H = -\frac{Ry}{n^2} \tag{1.1}$$

where $Ry = 13.6\text{ eV}$ is the Rydberg constant.

Alkaline atoms have many similarities with hydrogen. In highly excited alkalines the only electron in the outer shell is excited to a high energy state and travels in an orbit far from the nucleus that can reach few thousand times the radius of the ground state atom. The electron then feels the effect of the nucleus and the remaining electrons as

Property	Laws	Ground State	43S(tabulated)	70S(evaluated)
Binding energy	n^{-2}	4.18 eV	8.56meV	3.23meV
Orbit radius	n^2	5.632 a ₀	2384.2 a ₀	6317 a ₀
Polarizability	n^7	$-79.4 \text{ MHz}(\text{V cm}^{-1})^{-2}$	$-17,7 \text{ MHz}(\text{V cm}^{-1})^{-2}$	$-536.3 \text{ MHz}(\text{V cm}^{-1})^{-2}$
C_6	n^{11}	4707 au	$-1.697 \cdot 10^{19}$ au	$3611 \cdot 10^{24}$ au
Lifetime	n^3	— ^a	42.3 μs	195.8 μs
Level spacing ^b	n^{-3}	2.50 eV	100.5 GHz	23.3 GHz

^a For comparison we report lifetime of $5P_{3/2} = 26.2\text{ns}$

^b Level spacing are considered to the $n + 1$ state

Table 1.1: Scaling laws for the main properties of Rydberg atoms used in the text, tabulated values for the ground and 43S states from [7], and values for the 70S state evaluated with the application of the scaling laws to the tabulated values of the 43S state.

a single core similarly to the electron orbiting around the proton in the hydrogen. In the quantum defect theory the difference due to the presence of the core electrons can be reduced to a quantum defect $\delta_{n,j,\ell}$ that modifies the principal quantum number of the state. The high energy levels of alkaline atoms are then described by:

$$E_{Ryd} = \frac{Ry}{(n - \delta_{n,j,\ell})^2} \quad (1.2)$$

The quantum defect decreases with increasing principal quantum number [5], so that the hydrogen-like description becomes more appropriate for highly excited states. This description leads to the formulation of simple scaling laws for the properties of Rydberg atoms as a function of the effective quantum number $n - \delta_{n,j,\ell}$ [6]. This simple description makes of alkalines the most common candidate for Rydberg experiments. For illustration in Tab.1.1 we report the scaling laws of the properties used in the thesis and we use them to evaluate the properties of the 70S state, starting from the tabulated values for the 43S state [7]. In addition to show the stark difference of Rydberg levels from low levels we report the same properties for the ground state.

1.2 van der Waals interactions and dipole blockade

A large part of this thesis is dedicated to the study of many-body effects, which in our system are caused by van der Waals (vdW) interactions. Here we report a simple model explaining their origin [8].

We consider again the hydrogen-like representation of Rydberg atoms used in the previous section and suppose a neutral atom with core A and an electron 1 in a highly

excited state and a neutral atom with core B and an electron 2 in a highly excited state.

Two such atoms interact through an electro-magnetic potential that depends on the relative distance \mathbf{R} of the atomic cores and the positions of the electrons.

$$H_{AB} = \frac{e^2}{\mathbf{R}} - \frac{e^2}{\mathbf{r}_{A2}} - \frac{e^2}{\mathbf{r}_{B1}} + \frac{e^2}{\mathbf{r}_{12}} \quad (1.3)$$

We neglect the electron-electron interaction term and we expand the atomic position using:

$$\left(\|\mathbf{R} + \mathbf{r}\|^2\right)^{-\frac{1}{2}} = \frac{1}{R} \left(1 - \frac{\mathbf{n} \cdot \mathbf{r}}{R} + \frac{3(\mathbf{n} \cdot \mathbf{r})^2 - r^2}{2R^2} + \dots\right) \quad (1.4)$$

Here \mathbf{n} indicates the direction of \mathbf{R} . The interaction term of the Hamiltonian becomes in the second order expansion,

$$\frac{e^2}{R^3} (\mathbf{r}_{A1} \cdot \mathbf{r}_{B2} - 3(\mathbf{r}_{A1} \cdot \mathbf{n})(\mathbf{r}_{B2} \cdot \mathbf{n})) = \frac{\boldsymbol{\mu}_A \cdot \boldsymbol{\mu}_B - 3(\boldsymbol{\mu}_A \cdot \mathbf{n})(\boldsymbol{\mu}_B \cdot \mathbf{n})}{4\pi\epsilon_0 R^3} \quad (1.5)$$

where $\boldsymbol{\mu}_A$ and $\boldsymbol{\mu}_B$ are respectively the electric dipole operator of the atoms of core A and B and ϵ_0 the dielectric constant of vacuum.

In the absence of an electric field the atoms do not have a permanent dipole moment, but they can still interact through the exchange of excitation, originated by a transition dipole, corresponding to the atoms transition from state $|r\rangle$ to state $|r'\rangle$. The field radiated by such a transition corresponds to that of a classical dipole with moment $\boldsymbol{\mu}$ oscillating at frequency $\omega = (E_r - E_{r'})/\hbar$:

$$\mathbf{E}(t) = \mathbf{E}(\mathbf{R})e^{-i\omega t} \quad (1.6)$$

The field radiated by the atom A then interacts with the electrical dipole moment of atom B, and the interaction energy arising from this process is:

$$\mathbf{E}_A(t)\boldsymbol{\mu}_B(t) = \mathbf{E}_A(\mathbf{R})\boldsymbol{\mu}_B e^{-i(\omega_{k_A, k'_A} + \omega_{k_B, k'_B})t} \quad (1.7)$$

where $\mathbf{E}(\mathbf{R})$ is the electric field of the static dipole. This interaction exists even with non permanently polarized atoms. The interaction Hamiltonian can then be written as

the real part of Eq.1.7:

$$H_{12} = \text{Re}[-\mathbf{E}_A(\mathbf{R}) \cdot \boldsymbol{\mu}_B] = \quad (1.8)$$

$$\frac{1}{4\pi\epsilon_0} \left\{ [\boldsymbol{\mu}_A \cdot \boldsymbol{\mu}_B - 3(\mathbf{n} \cdot \boldsymbol{\mu}_A)(\mathbf{n} \cdot \boldsymbol{\mu}_B)] \left(\frac{\cos(kR)}{R^3} + \frac{k \sin(kR)}{R^2} \right) \right\} + \quad (1.9)$$

$$\frac{1}{4\pi\epsilon_0} \left\{ [\boldsymbol{\mu}_A \cdot \boldsymbol{\mu}_B - (\mathbf{n} \cdot \boldsymbol{\mu}_A)(\mathbf{n} \cdot \boldsymbol{\mu}_B)] \frac{k^2 \cos(kR)}{R} \right\} \quad (1.10)$$

where $k = \omega_{r_1 r'_1} / c$ is the wave number of the radiated field.

The corresponding quantum hamiltonian has a similar form with quantum electrical dipole moment operator $\boldsymbol{\mu}_i^{r_i r'_i} = \langle r_i | \mathbf{d} | r'_i \rangle | r'_i \rangle \langle r_i |$ replacing the classical electrical dipole moment.

The total Hamiltonian for the two interacting atoms can be written in the basis of states $|r'_1, r'_2\rangle, |r_1, r_2\rangle$ as:

$$\begin{pmatrix} \hbar\Delta & V \\ V & 0 \end{pmatrix} \quad (1.11)$$

where $V = \langle r_1 r_2 | H_{12} | r'_A, r'_B \rangle$ and $\hbar\Delta = (E_{r'_1} + E_{r'_2}) - (E_{r_1} + E_{r_2})$ is the Förster energy mismatch.

The interaction term V can be written as C_3/R^3 where C_3 derives from the Clebsch-Gordan coefficients. The eigenstates of the Hamiltonian 1.11 have eigenenergies

$$\hbar\tilde{\Delta}(r_{AB}) = \frac{\hbar\Delta}{2} - \text{sign}(\hbar\Delta) \sqrt{\frac{\hbar^2\Delta^2}{4} + \left(\frac{C_3}{R^3}\right)^2} \quad (1.12)$$

From the eigenenergies it is possible to define a characteristic distance R_{vdW} from the relation:

$$\hbar\Delta = \frac{C_3}{R_{vdW}^3} \quad (1.13)$$

when $r_{AB} \gg R_{vdW}$ the energy shift can be written as:

$$\Delta E \sim \frac{(C_3/R^3)^2}{\hbar\Delta} = \frac{C_6}{R^6} \quad (1.14)$$

which is the regime of van der Waals forces. In Rydberg atoms, the high electrical polarizability confers to the atoms a large dipole moment, thus an high C_6 coefficient. Thus van der Waals interactions make the atoms strongly interacting, and permit the emergence of strong many-body effects.

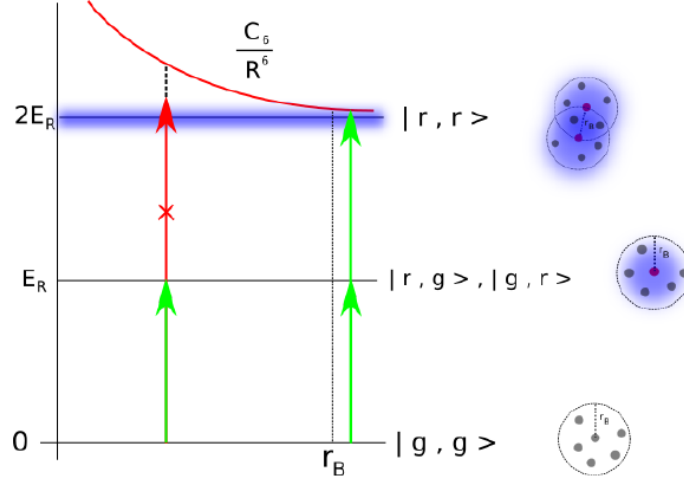


Figure 1.1: In the blockade effect the van der Waals interactions shift the energy of the symmetric state $|r'r'\rangle$ by $\hbar\delta = C_6/r^6$. When the shift is greater than the Rabi frequency, the excitation of the second atom is off-resonant and, hence, strongly suppressed.

Suppose now that the two atoms are irradiated with a resonant transition with Rabi frequency Ω and let assume that one of the two atoms is excited to the Rydberg level. In this condition if also the second atom were excited to Rydberg level the two atoms would be in the symmetric excited state $|r'_1, r'_2\rangle$, whose energy would be shifted by $\Delta E = C_6/R^6$. When the interaction energy becomes larger than the Rabi Frequency the transition to the symmetric state is out of resonance and the excitation of the second atom is suppressed, so that only one atom at a time can be excited to Rydberg state (Fig.1.1). This effect is known as the *blockade effect*.

In a fully coherent picture with two indistinguishable atoms initially in the ground state, there is no way of knowing which of the two atoms has been excited to the Rydberg state, so that the system is better described as a coherent superposition, called *superatom*, of the two possible states with one atom in the excited state and the other in the ground state. Blockade effect and superatom constitute one of the most peculiar behaviors of Rydberg atoms.

1.3 Coherent and Incoherent regimes

We now want to observe how the system can evolve under the action of a resonant radiation of frequency ω .

To do so we consider the atom as a two level system with a ground state $|g\rangle$ and an excited state $|e\rangle$. In the case that the system is perfectly closed so that there are no losses and the radiation is coherent, the dynamics of the system is characterized by a harmonic oscillation between ground and excited state at the Rabi frequency Ω

$$\Omega = \frac{d \cdot E}{\hbar} \quad (1.15)$$

where d is the dipole matrix element between the ground and the excited state and E the field of the radiation. In the experiment the losses from the excited level reduce the coherence of the system and thus a complete description requires the formalism of the density matrix:

$$\rho = \begin{pmatrix} \rho_{gg} & \rho_{ge} \\ \rho_{eg} & \rho_{ee} \end{pmatrix} \quad (1.16)$$

To find the solution of the system we solve the time dependent Schrödinger equation

$$i\hbar \frac{d}{dt} \rho = [H; \rho] \quad (1.17)$$

for the Hamiltonian

$$H = E_g |g\rangle \langle g| + E_e |e\rangle \langle e| - \frac{\hbar\Omega_0}{2} e^{-i\omega_L t} |g\rangle \langle e| - \frac{\hbar\Omega_0}{2} e^{+i\omega_L t} |e\rangle \langle g| \quad (1.18)$$

Eq.1.17 provides the Optical Bloch Equations of the system. By introducing the population difference $w = \rho_{ee} - \rho_{gg}$ and the coherence $\tilde{\rho}_{eg} = e^{i\omega t}$, the Optical Bloch Equations in the rotating wave approximation can be cast in the simple form:

$$\begin{cases} \frac{d}{dt} \tilde{\rho}_{eg} = -(\gamma_{\perp} - i\delta) \tilde{\rho}_{eg} + \frac{i\Omega_0}{2} w \\ \frac{d}{dt} w = -\gamma_{\parallel} (w + 1) - i\Omega_0 (\tilde{\rho}_{eg} - \tilde{\rho}_{ge}) \end{cases} \quad (1.19)$$

In the equations we introduced two relaxation terms γ_{\parallel} and γ_{\perp} , the first accounts for the relaxation of the populations given by spontaneous emission, while the second introduces a dephasing of the coherences.

The equation can be solved in the adiabatic approximation that assume that the population evolves at a much slower rate than the coherences, thus $\gamma_{\parallel} \ll \gamma_{\perp}$. In this

approximation we can deduce the rate to reach the stationary state:

$$\Gamma = \gamma_{\parallel} + \gamma_{\perp} \frac{\Omega^2}{\gamma_{\perp}^2 + \delta^2} \sim \Omega^2/\gamma_{\perp} \quad (1.20)$$

where δ is the detuning of the radiation from resonance. This rate distinguishes two typical types of behavior of the system: in the coherent regime $\Omega^2/\gamma_{\perp} \gg 1$ the system evolves coherently and the excitation probability depends linearly on the Rabi frequency ($\propto \Omega t$); in the incoherent regime $\Omega^2/\gamma_{\perp} \ll 1$ the system evolves classically and the excitation probability depends quadratically of the Rabi frequency ($\propto \Omega^2 t$). The results of this thesis are mainly obtained in the incoherent regime, but few hints of coherent dynamic will be given in Sec.4.3.

1.4 Resonant and off-resonant excitation dynamics

We observed in Sec.1.2 that when the frequency shift due to van der Waals interactions is bigger than the Rabi frequency, the excitation of other atoms is suppressed. In the coherent regime this condition defines a characteristic distance r_B , called *blockade radius*, that represents the minimum distance at which two atoms can be excited by a resonant radiation

$$\frac{C_6}{R^6} = \hbar\Omega \quad (1.21)$$

In the incoherent regime $\gamma \gg \Omega$, there is a similar effect that arises from a classical local excitation rate:

$$\Gamma_i(\Delta) = \frac{\Omega^2}{2\gamma} \left[1 + \left(\frac{\Delta - \frac{1}{\hbar} \sum_{i \neq j} V_{ij} n_j}{\gamma} \right)^2 \right]^{-1} \quad (1.22)$$

where V_{ij} is the interaction potential due to van der Waals interactions and Δ the detuning with respect to resonance. For $\Delta = 0$ the proximity of an excited atom suppresses the excitation rate and leads to the *blockade constraint* [9, 10], with a characteristic distance:

$$r_b = \left(\frac{C_6}{\hbar\gamma} \right)^{\frac{1}{6}} \quad (1.23)$$

It follows directly from Eq.1.22, that as the number of excitations grows in an area, the local excitation rate decreases, causing a slow down of the dynamics.

A completely different dynamics arises when the laser is detuned by an amount Δ with respect to the resonant transition. If the detuning has the same sign as the energy shift

due to van der Waals interactions, it can compensate the shift and excite resonantly atoms at $r < r_b$ [11, 12]. In this case the distance of excitations r_{fac} is determined by the detuning of the laser through the resonant condition:

$$\frac{C^6}{r_{fac}^6} = \hbar\Delta \quad (1.24)$$

The finite linewidth of the laser makes available a whole *facilitation shell* around r_{fac} of width

$$\delta R_{fac} = \frac{1}{2} r_{fac} \frac{\delta_L}{\Delta} \quad (1.25)$$

Since an excitation created through this process can, in turn, facilitate the excitation of further atoms, the off-resonant excitation leads to avalanche processes that determine the formation of clusters of Rydberg atoms. A thorough theoretical description of the cluster formation can be found in [9], while a detailed experimental study is presented in [11]. In this thesis we limit ourselves to a simple heuristic description.

The cluster formation needs an initial single excitation called *seed* that can be created either – albeit with a low probability – spontaneously, by the off-resonant radiation or artificially by exciting a few atoms through a brief resonant laser pulse [13]. The seed determines a facilitation shell around itself, so that the second atoms is then excited resonantly at the distance r_{fac} from the seed. The next atom can be created in a facilitation volume that is composed by all the points at distance $R = r_{fac}$ from one of the two atoms minus a small area in which the facilitation shells overlap as described in Fig.1.2, therefore there is a larger available volume for the excitation. In 2-dimensional and 3-dimensional geometry, for each new excitation the total volume occupied by all excitation shells increases, thus enhances the probability of the next excitation giving rise to an avalanche process. In a 1-dimensional geometry the total facilitation volume is always given by part of the facilitation shell of the two extremal atoms of the cluster. 1-dimensional clusters of atoms created by off-resonant excitation have a well defined interaction energy, due to the regular spacing of atoms r_b . In the 2-dimensional and 3-dimensional configuration the higher number of neighbours complicates the energy distribution.

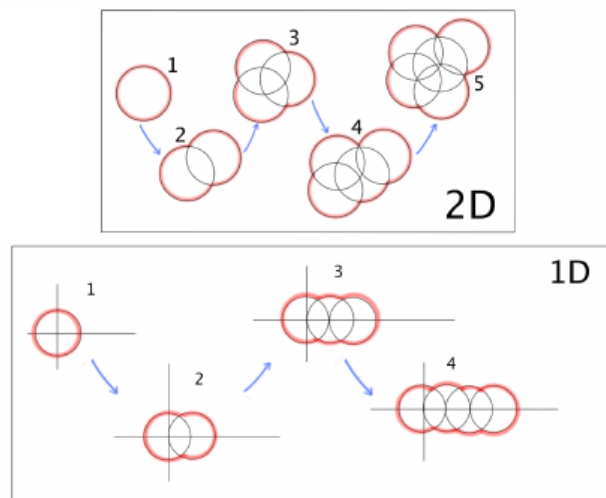


Figure 1.2: In the off-resonant excitation dynamics, the detuning of the laser compensates the energy shift due to van der Waals interactions for a specific distance, r_{fac} , for which the excitation becomes facilitated. After the first excitation, for each successive excitation the facilitation volume increases and consequently increases the probability of exciting another atom. The avalanche process gives rise to clusters of Rydberg atoms with atoms spacing r_b .

Chapter 2

Experimental apparatus

2.1 Overview

The main purposes of the experimental apparatus are to trap the ground state atoms, excite them to Rydberg states and eventually detect Rydberg atoms. Each of these functions requires dedicated technology and entails specific problematics. This chapter reports only a brief overview of the main processes and technology involved, sufficient to give the reader the necessary background to appreciate the content of the thesis, while for a more detailed description we refer the reader to [14]

2.2 Magneto Optical Trap

The first step in the experiment is to cool and to confine a cloud of rubidium atoms, so that we can easily access and manipulate them. In order to do so, we need a force that acts on the atoms and that is velocity dependent to slow down, hence cool, the atoms and space dependent to confine them. In our experiment we use a magneto optical trap (MOT), which combines the action of the optical beams which exert the force and slow down the atoms, with a magnetic field that makes the force space dependent.

The basic principle of the trap can be easily explained in a 1-dimensional system and then extended to the 3-dimensional case.

Initially, to understand the force that acts on the system, we consider an atom at rest irradiated by a radiation of frequency ω . The atom is described as a two-level system with ground and excited state separated in energy of $\hbar\omega_0$. When the atom absorbs a photon from the beam it receives a momentum $\hbar k$ in the direction opposite to the

beam source. The photon can be re-emitted in two ways:

- by induced emission the atom emits a photon identical to the ones of the beam, so it receives a recoil momentum $-\hbar k$. After the emission the atom will be back in the initial conditions as the total pulse received is $\hbar k + (-\hbar k) = 0$
- by spontaneous emission the atom emits the photon in a random direction, so it receives a recoil momentum $\hbar k'$. After the emission, the momentum from spontaneous emission averaged over numerous repetitions gives a null contribution to the atom motion.

The unbalanced motion due to the spontaneous emission is associated to a radiation pressure force. This pressure is at the root of our trapping technique.

The next step in understanding the MOT is to see how the radiation pressure can be velocity selective. In a one directional system consider an atom moving toward the source with speed v_{at} . In the coordinate system of the atom, the source is moving at $-v_{at}$ so that the photons are shifted in frequency due to Doppler effect by an amount $\delta\omega_{rad} = kv_{at}$. We can use the Doppler shift to make the absorption velocity selective. For example by using a light source that is red detuned with respect to the atomic transition of the atom at rest, we are resonant only if the atom is moving toward the source at a velocity such that the Doppler shift compensates the detuning $kv_{at} = \omega_{rad} - \omega_0$. When the resonance condition is matched the atom absorbs photons from the source and it slows down under the action of the radiation pressure. However as the atom slows down the Doppler shift changes and the Doppler shifted photons of the source will not be resonant anymore with the atomic transition. We need then to extend the resonant condition so that it is matched for a bigger range of velocities and we need to introduce a space dependent mechanism.

We now show that these results can be achieved with the introduction of a magnetic sub-level and an appropriate choice of the beam polarizations.

For simplicity consider that the ground state has hyperfine momentum $F=0$ and that the excited state has $F=1$, so it has Zeeman degenerate sub-levels $m_F = +1$, $m_F = 0$, $m_F = -1$. Then if we apply a circularly polarized light σ^+ we address in the excited state only the $m_F = +1$ Zeeman sub-level, while for σ^- only the $m_F = -1$ Zeeman sub-level is coupled to the ground state. To establish a notation convention, we suppose that the beam propagates along the axis \hat{x} and that the atom is moving along the same

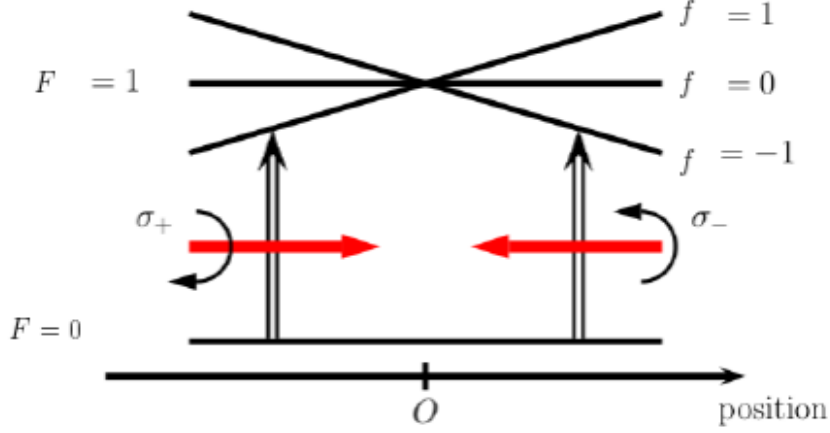


Figure 2.1: In the MOT the magnetic field shifts the Zeeman sub-levels of the atoms. The two beams are resonant only in a specific region of the space and exert a pressure toward the center of the trap.

axis. If we now apply a space dependent magnetic field with a zero crossing:

$$B = -bx\hat{z} \quad (2.1)$$

the field removes degeneracy of the Zeeman sub-levels that are shifted by the Zeeman effect

$$\delta E = -m_F g_L \mu_B \cdot bx \quad (2.2)$$

where $-g_L$ is the Landé factor and μ_B the Bohr magneton.

The sublevel $m_F = 1$ is shifted toward higher energy for $x > 0$ and to lower energy for $x < 0$ and vice versa for $m_F = -1$ as shown in Fig.2.1. So if we send red detuned light with σ^+ polarization from the $-\hat{x}$ direction it is resonant only for $x < 0$ and it exerts a force toward the zero of the field, while for $x > 0$ the $m_F = 1$ is far from resonance due to the Zeeman shift. On the contrary σ^- light is resonant only for $x > 0$ and exerts a force toward the zero of the field. The radiation pressure, therefore, pushes the atoms always toward the zero of the field. To extend the MOT mechanism in three dimension it is sufficient to apply three orthogonal pairs of counter propagating beams with opposite polarizations and to apply an appropriate magnetic field that has a zero crossing in the center along all possible directions. In the experiment we use two MOT configuration, initially a two-dimensional MOT, created with two pairs of counter propagating beams and two pairs of coils in anti-Helmholtz configuration, collects the flux of atoms from the dispenser. Then the atoms are transferred to a three-dimensional

(3D) MOT, created with three pairs of counter propagating beams and three pairs of coils in anti-Helmholtz configuration. Both MOTs work on the atomic transition $5S_{1/2}, F = 2 \rightarrow 5P_{3/2}, F = 3$, driven by a slightly detuned laser with $\Delta = -2.9\Gamma$, in which $\Gamma = 6.055$ MHz is the linewidth of the laser. As we will see more in detail in Sec.3.1 the atoms can also be excited to the $5P_{3/2}, F = 2$ level from where they can leave the cooling transition. This loss channel is prevented with the introduction of an additional laser, called *repump laser*.

The magnetic field of the 3D MOT is provided by three pairs of coils in anti-Helmholtz configuration, which generate a gradient of 12.2G/cm. The final temperature of atoms is given by the Doppler limit $\sim 150 \mu\text{K}$. Typical sizes of the trapped cloud are $150 \mu\text{m}^3$. To prevent population of the 5P level during the excitation of Rydberg atoms, thus the introduction of a third level in the excitation dynamics, the laser beams of the MOT are turned off during the experiment. The MOT then expands due to thermal motion and falls under gravity. Due to the low thermal velocity $120 \text{ nm}/\mu\text{s}$ both effects are neglected in the initial part of the thesis where the experiment lasts for less than $15 \mu\text{s}$. A characterization of the changes in the cloud due to the turn off of the beams is presented in Sec.6.1.

The centers of the 2D and 3D MOTs are located in two vacuum chambers made of quartz. The vacuum pressure inside the two cells is kept respectively at 10^{-7} mbar and 10^{-10} mbar. The density of the trapped cloud and the dimension of the cloud are observed through the fluorescence signal. A CCD camera provides real-time imaging of the trapped cloud, while an high resolution camera ($3.3 \mu\text{m}$ per pixel) provides static images for the extrapolation of the cloud characteristics. Both cameras capture only the x, z plane of the MOT, where x is the direction of propagation of the excitation beams and z is the vertical axis. Processing of the high resolution imaging allows us to retrieve the MOT dimensions along the two axes, while the third dimension is estimated as

$$\sigma_y = \sqrt{\sigma_x \sigma_z} \quad (2.3)$$

A calibration, based on the fluorescence intensity, permits also to evaluate the total number of atoms N contained in the MOT with an error of 20%. From the total number of atoms and the dimensions of the MOT along the three axis we can evaluate the peak density as:

$$n = \frac{N}{\pi^{3/2} \sigma_x \sigma_y \sigma_z} \quad (2.4)$$

Typical densities of ground state atoms used in this thesis are $10^{10} - 10^{11}$ atoms/cm.

In the remainder of this thesis we will use the term MOT to refer by extension also to the trapped cloud as there will be no ambiguity of significance.

2.3 Excitation

In this thesis we study Rydberg S-states, i.e., having zero angular momentum, which due to their spherical symmetry have simple interaction properties [15]. However single photon excitation from the ground state $5S_{1/2}$ does not allow one to reach S-state. In addition single photon excitation to a Rydberg level would require laser light in the ultra-violet region that are difficult to obtain [7]. So it is easier to introduce an intermediate level in the excitation, that permits to use sources in the visible or IR region, for which there is a wide choice of sources, and at the same time enables excitation to S or D states. An example of such scheme is:

$$5S_{1/2} \rightarrow 6P_{3/2} \rightarrow 70S \quad (2.5)$$

in which the lower transition $5S_{1/2} \rightarrow 6P_{3/2}$ is driven by a blue laser at 421nm, and the upper transition $6P_{3/2} \rightarrow 70S$ by an IR laser at 1012nm. For the sake of simplicity of interpretation of the dynamics, we would like to neglect the intermediate state and consider the entire excitation as a single transition $5S_{1/2} \rightarrow 70S$. This is possible only if the intermediate state does not get populated. By detuning the intermediate state from the 6P level by δ_{6p} we are able to reduce population of the 6P level and favour the two-photon transition through a virtual level over the two-step transition. When the population of the 6P state can be neglected the two-level model can be applied. The correct transition is represented in Fig.2.2. In Fig.2.2 we also include the possibility of a detuning Δ from the Rydberg state that will be used in Sec.5.3 to perform off-resonant excitation. Determining the conditions for which the two-level approximation is justified is one of the results of this thesis and will be discussed in detail in Sec.3.2.1 and Sec.4.2.

In the two level approximation it is useful to introduce also the effective Rabi Frequency of the two-photon process:

$$\Omega_{2ph} = \frac{\Omega_{blue}\Omega_{IR}}{2\delta_{6p}} \quad (2.6)$$

Where Ω_{IR} and Ω_{blue} are respectively the Rabi frequency of 421 nm laser and 1012 nm laser.

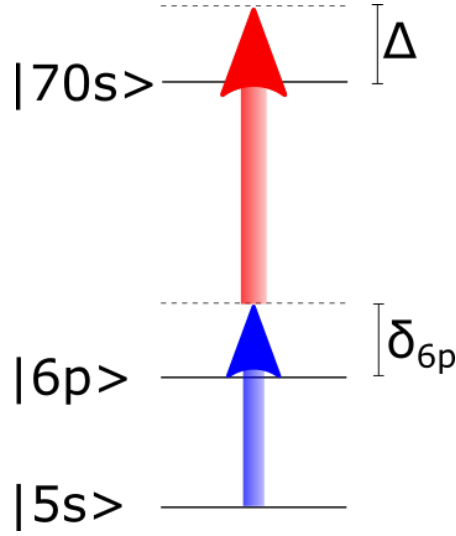


Figure 2.2: We excite the atoms from the ground state $5S_{1/2}$ to the Rydberg state $70S_{1/2}$ with a two-photon excitation scheme, via a virtual level. We can perform resonant excitation with the total frequency matching the energy difference between the two levels, or off-resonant excitation detuned by Δ from the Rydberg state. The virtual level is detuned by δ_{6P} from the $6P_{3/2}$ state.

To be able to perform two-photon excitation from a more practical point of view we need the two beams to be overlapped and to overlap with the atoms in the MOT. The overlap of the three (blue and IR beam and MOT) defines the effective volume of the experiment and discriminates between the one dimensional and three dimensional geometry of the sample we are about to describe.

The blue and IR beam are in co-propagating configuration and propagate in the MOT along the \hat{x} direction, so the effective volume can be evaluated considering a cylinder of radius equal to the smaller of the two waists w and length equal to the length of the MOT in that direction:

$$V = \pi w^2 \sigma_x \quad (2.7)$$

The 1012 nm laser has always $w_{IR} = 130 \mu\text{m}$ while the 421 nm laser can have $w_{Blue} = 45 \mu\text{m}$ or $w_{blue} = 6 \mu\text{m}$. In the former case we have a 3D configuration, while in the latter case the radial dimension of the effective volume is smaller than the blockade radius, hence multiple excitations in the radial dimension are strongly suppressed and the sample assumes a quasi-1D configuration.

Up to now we discussed the overlap of the beams in space. Overlap in time is just as essential and requires good timing and fast switching of the beams. Blue and IR beams

are turned on $5\ \mu\text{s}$ after the trap beams are turned off, so to allow for all atoms in the $5P$ state to decay back to the ground state ($t_{life}(5P) \sim 30\ \text{ns}$). Typical excitation pulses used in this thesis last $\tau_{exc} \leq 10\ \mu\text{m}$. The fast switching of the laser beams is achieved with the use of acousto-optical modulators. In an acousto-optical modulator a crystal is crossed by an acoustic wave, which excites collective modes in the crystal. When the light crosses the crystal phonon-photon scattering processes are possible and the beam is diffracted according to the Bragg laws:

$$k' = k_0 + k_{RF} \quad \omega' = \omega_0 - \omega_{RF} \quad (2.8)$$

In the above equation k_0 and ω_0 are the initial wave vector and frequency of the photon, while k_{RF} and ω_{RF} are those of the radio frequency (RF). Thanks to an absorber, put on the opposite side of the antenna source of the RF wave in the AOM, the waves do not bounce back after crossing the crystal, so that k_{RF} phonons are directed always from the antenna to the absorber.

Then at the output of the AOM we will find non scattered photons, corresponding to the zero order of diffraction, photons associated to the absorption of a phonon that create the +1 order of diffraction and photons associated with emission of a phonon that create -1 order of diffraction, successive orders of diffraction that can be obtained by multiple scattering.

The on-off switching time of the diffracted beam is determined mainly by the time takes to cross the crystal and is usually about $t_{AOM} \sim 100\ \text{ns}$. Thus by using as excitation beam the first diffracted order of the AOM we are able to switch on and off the beams on that time scale.

Satisfaction of the Bragg laws (Eq.2.8) can not be achieved simultaneously for all diffraction orders. The angle between the incident light and the direction of propagation of the RF, determines the diffraction efficiency of each order. This permits us to optimize the alignment to obtain the maximum diffraction efficiency on the order we require in the experiment.

From the Bragg diffraction laws it follows that keeping the same angle between the RF and the beam and changing the radio frequency changes both the diffraction angle and the diffraction efficiency. To avoid the former we use double pass configuration shown schematically in Fig.2.3. Calling y the propagation direction of the radio frequency, the beam is initially perpendicular to the acoustic wave so with momentum 0 along y . The first diffracted order, therefore, gains momentum $\hbar k$ along y . After the AOM only

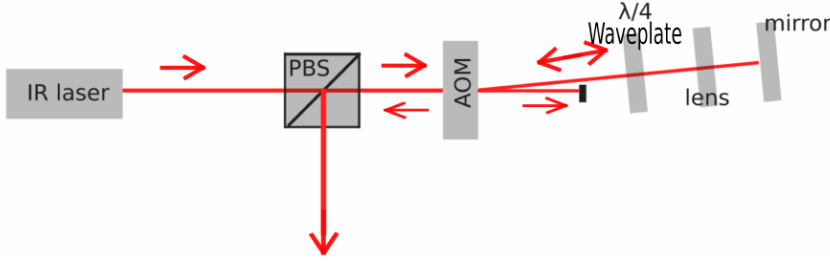


Figure 2.3: Scheme of the double passage configuration of the AOM. In the AOM a RF-frequency diffracts the beam accordingly to Bragg laws. In the double passage the diffracted beam is reflected on its self and crosses again the AOM. In this configuration the output angle does not depend on the RF-frequency. The total shift in frequency of the beam is twice the applied RF-frequency.

the first diffracted order is reflected on its path and when it crosses again the AOM it has momentum $-\hbar k$ along y , then its $+1$ diffracted order that gains again momentum $\hbar k$ has momentum 0 along y , independently of the applied radio frequency.

The $+1$ diffracted order of the second passage is overlapped with the original beam before the AOM. In order to separate the two beams we polarize the light that goes through the AOM and we use a double passage through a $\lambda/4$ plate to rotate the polarization by $\pi/2$. In this way the two beams can be separated with the use of a polarizing beam splitter. The double passage has also the advantage of doubling the frequency change allowed by the AOM as the first diffracted order of the reflected beam has $\omega = \omega_0 + 2\omega_{RF}$, however it has the disadvantage of doubling the change in efficiency of the AOM with the frequency, this problem is dealt with in Sec.4.1.

2.4 Detection

Rydberg atoms are neutral atoms and thus it is difficult to detect them directly, on the other hand ions are easy to detect and Rydberg atoms can be easily ionized thanks to the low ionization energy:

$$E_{ion} = \frac{Ry^2}{4k(n - \delta_{n,j,l})^4 e^3} \quad (2.9)$$

where Ry is the Rydberg constant $Ry = 13.3 \text{ eV}$, e the electron charge, $k = 1/4\pi\epsilon_0$ and $n - \delta_{n,j,l}$ is the effective n-quantum number of the state. For the 70S state used in this thesis $E_{ion} \sim 16 \text{ V/cm}$

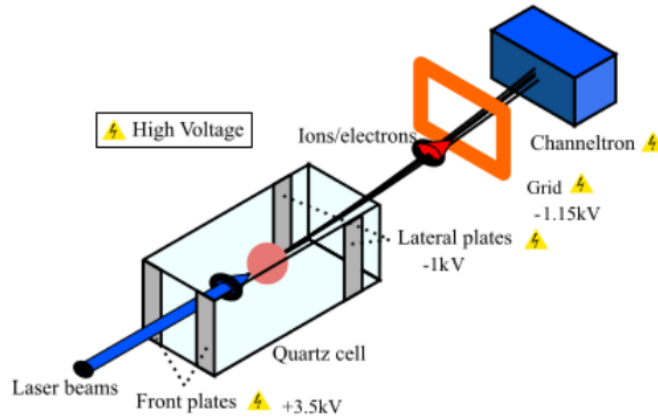


Figure 2.4: In our detection apparatus two pairs of electrical plates apply an high voltage field to the sample that ionize all Rydberg atoms with $n \gtrsim 40$. The grid accelerates the ions toward the channeltron, that detects them.

In the experiment the field is provided by two pairs of copper electrical plates, mounted on the sides and on the front of the cell. The electric field applied to the plates (3.5 kV on the frontal ones and 1kV on the lateral) ionizes all Rydberg states with $n \gtrsim 40$. After ionization there is no way to discriminate the ions based on the initial Rydberg state, hence this technique is called non-selective field ionization.

In the detection process, after ionization, a grid accelerates the ions toward the detector as shown schematically in 2.4. Ion detection is performed by a channel electron multiplier (Channeltron). When the ions hit the surface of this device they release electrons that are accelerated toward the inner part of the detector. These electrons, in turn, will hit the detector walls, releasing other electrons in an avalanche process. The electronic signal that reaches the inner part of the detector is processed by an oscilloscope with high sampling speed.

Fig.2.5 shows an example of the channeltron output on the oscilloscope. Each peak corresponds to a single ion hitting the detector surface, and the different heights of the peaks depend on the efficiency of the amplification process in the channeltron. The arrival times hold information on the spatial distribution of the Rydberg atoms [12]. The ions are counted through a peak counting routine that resolves peaks with at least 10 ns separation and set an upper limit to 30-40 detectable excitations. The total

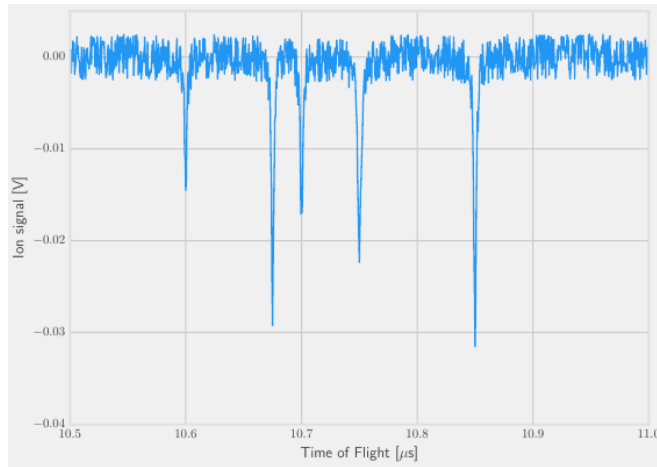


Figure 2.5: The signal of the channeltron is fed to an oscilloscope with high acquisition rate, in the oscilloscope output each peak corresponds to the arrival of an ions. The arrival time on the x-axis depends linearly on the position. The amplitude of the peaks depend on the gain of the channeltron.

detection efficiency of the apparatus is $\eta = 0.4 \pm 0.1$ [16]

The trap excitation and detection cycle is repeated at a rate of 4 Hz. The choice of this repetition rate is mainly determined by the need to prevent accumulation of charges on the quartz cell [17]. The measurements reported in this thesis represent statistical averages over typically 100 repetitions of the experimental cycle of which we report the average value and, where appropriate, we also report the standard error defined as the ratio of the standard deviation (measured from the experiment) over the square root of the number of repetition.

Chapter 3

Multi-level effects

3.1 Multi-level in low lying states

The purpose of this chapter is to introduce multi-level phenomena in Rydberg atoms, however before discussing the effects on Rydberg atoms, we consider useful to introduce multi-level effects in low lying states. The reason of this deviation is that in low lying states such effects are well known and a specific technique has been introduced to circumvent them. The example we report here is of laser cooling and repump laser, both fundamental to the MOT.

In the typical laser cooling scheme for Rb in MOT (Fig.3.1), the laser drives the transition $5S_{1/2}, F = 2 \rightarrow 5P_{3/2}, F = 3$. Atoms in the $5P_{3/2}, F = 3$ level decay spontaneous only to the $5S_{1/2}, F = 2$ level and remain in the cooling transition. Thus cooling, so far, is a close two-level process.

However it is possible to excite off-resonantly atoms to the $5P_{3/2}, F = 2$ level, from where they decay spontaneously not only to the $5S_{1/2}, F = 2$ level, but also to the $5S_{1/2}, F = 1$ level. Atoms in the $5S_{1/2}, F = 1$ level can not be excited back to the $5P_{3/2}, F = 2$ level, hence they are lost to the cooling transition and escape the trap. Knowing exactly which levels out of the cooling transition are populated makes it possible to circumvent the problem. By addition of a laser to drive the $5P_{3/2}, F = 2 \rightarrow 5S_{1/2}, F = 1$ transition, we can bring atoms back in a level involved in the cooling transition. This laser is called repump laser and is a fundamental in most cold atoms experiments.

During my thesis I was hosted for two months in the 5th Physikalisches Institute of Stuttgart University where I had the chance to cooperate to the set-up of a repump laser for Rb and take a deeper look at the technique application. The main results

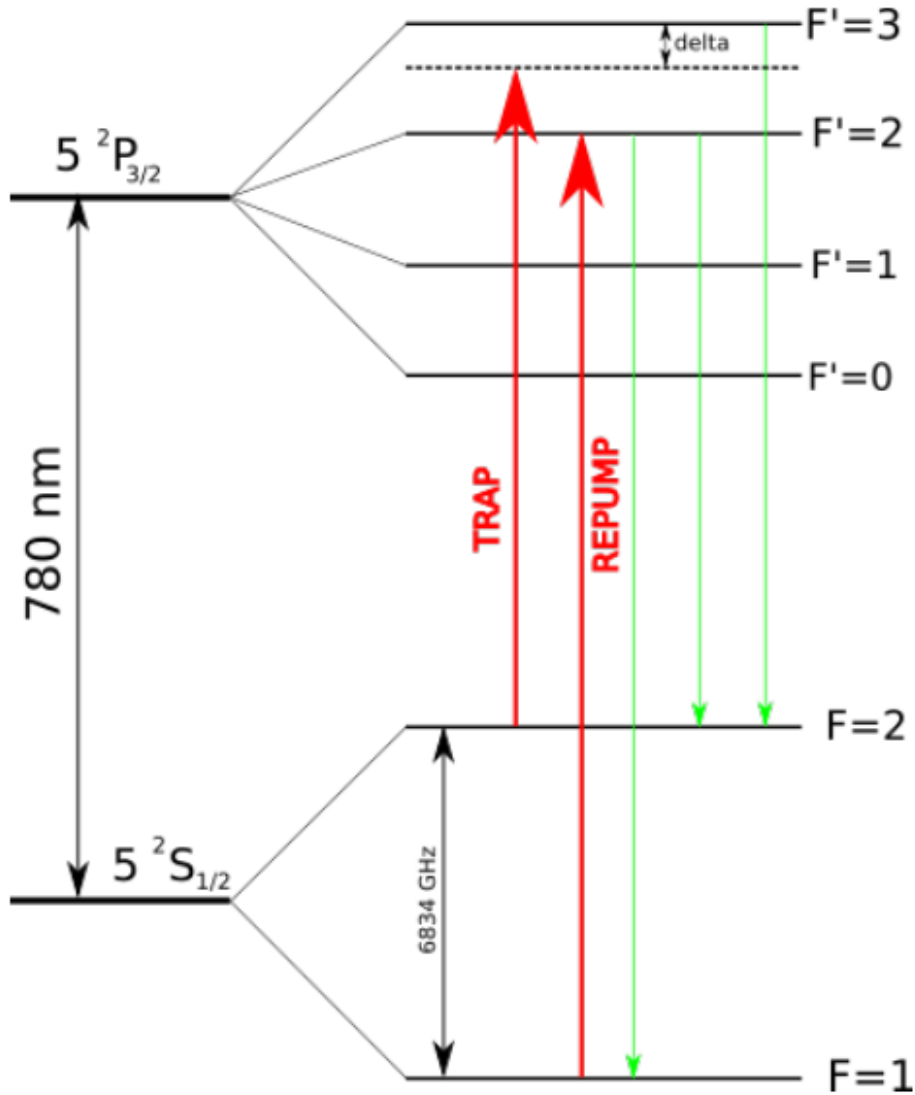


Figure 3.1: Scheme of the levels involved in the cooling and the repump transitions. The cooling drives resonantly the $5S_{1/2}, F = 2 \rightarrow 5P_{3/2}, F = 3$ transition and off-resonantly the $5S_{1/2}, F = 2 \rightarrow 5P_{3/2}, F = 2$. Both atoms in the $5P_{3/2}, F = 3$ level and those in the $5P_{3/2}, F = 2$ level decay spontaneously to the $5S_{1/2}, F = 2$ level, but atoms in the $5P_{3/2}, F = 2$ level, also decay to the $5S_{1/2}, F = 1$ level, which is out of the cooling transition. The repump laser collects the atoms in the $5S_{1/2}, F = 1$ level and excites them to the $5P_{3/2}, F = 2$ state from where they can re-enter the cooling transition.

obtained contextually to this experience are reported in Appendix A.

3.2 Multi-level effects in Rydberg states

3.2.1 6p hyperfine structure

In Sec2.3 we saw that to reach Rydberg level, we use a two-photon process through a virtual level. The purpose the virtual level, that by definition is never populated, is to simplify the interpretation of the excitation dynamics by removing the intermediate level from the model. However to induce a dipole moment on the virtual level we need a real level. Therefore in our scheme, the virtual level is close in energy to the $6P_{3/2}$ level. In this configuration population of the $6P_{3/2}$ level is not only possible, but in some cases it is also very likely. So when the 6P level is populated the system acquires an intermediate level and the two-level model can not be applied to the description of the excitation. Deviations from the two-level model are particularly evident when more than one sub-level of the 6P state get populated.

Potential population of the $6P_{3/2}$ state during excitation is due to the characteristic of the lower transition laser (detuning and power). Suppose now to chose for the power and the detuning of the blue laser values that causes population of one or more hyperfine sub-levels of the $6P_{3/2}$ state. The hyperfine sub-levels of the $6P_{3/2}$ state are some tens MHz apart. Now we scan with the frequency of the IR laser the frequency region around the expected two-photon transition. The spectrum obtained in this way will have several peaks corresponding to the resonant transition *sub-level* \rightarrow *Rydberg* from different sub-levels of the $6P_{3/2}$ state, to the same Rydberg level. Thus population of the 6P level induces a structure on the Rydberg spectra. In the experiment we observe such structure.

We used the 421nm laser with a red detuning with respect to $6P_{3/2}, F = 3$ sub-level, so that its frequency is close to the lower hyperfine sub-levels, across the expected frequency range for the two-photon transition. The blue pulse and IR pulse are synchronous and last $t_{exc} = 1 \mu s$ Fig.3.2 shows the number of Rydberg atoms detected as a function of the IR laser frequency with respect to the expected two-photon transition. In the spectra we resolve three different peaks with different amplitudes, from a fit to three Gaussian we obtain the centers of the curves: 1, 37 MHz, -76 MHz, and -170 MHz. While the theoretical splitting of the hyperfine sub-levels of the $6P_{3/2}$ level is starting from the $6P_{3/2}, F = 3$ sub-level: 0 MHz, -87 MHz, -138 MHz [18]. The difference between the two spectra is probably explained in terms of the Autler Townes splitting on the three sub-levels, but it is not investigate in this thesis. Instead we want

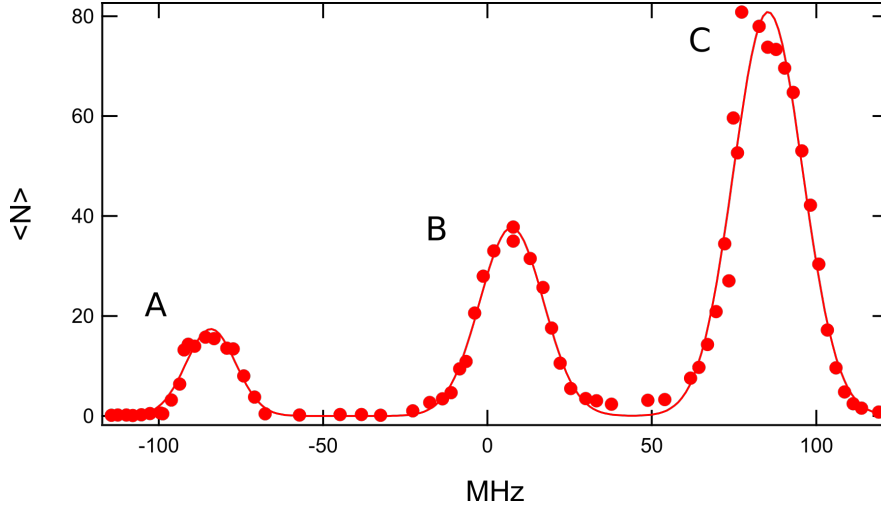


Figure 3.2: Two steps excitation can populate different $6P_{3/2}$ hyperfine sub-levels. This structure emerges on the Rydberg spectrum as it creates different pathways to reach the same state $70S$.

to stress that the structure of the intermediate state, when it is populated, induces a structure in the Rydberg spectra due to the different pathways to reach the Rydberg state. This structure is clearly incompatible with the two-level model.

Ideally to remove the emergence of such structure in the Rydberg spectrum, we would like to avoid completely population of the $6P_{3/2}$ state, hence the $6P_{3/2}$ hyperfine structure. This means performing a perfect two-photon transition.

As we will see during this thesis (Sec.4.2) this is not possible in absolute terms, but just by applying a few expedients it is possible to reduce the population of the $6P_{3/2}$ level, so that we can neglect its effects. The first of this expedient is to use a blue detuning with respect to the upper hyperfine sub-level of $6P_{3/2}$, that is $6P_{3/2}, F = 3$. In this way the population of the lower hyperfine sub-levels is suppressed as radiation is far off-resonant. However as we will see in Sec.4.2 population of the $6P_{3/2}, F = 3$ sub-level is still significant to the technique we want to apply.

3.2.2 State transfer from black body radiation

In Sec.3.1 while examining multilevel effects on the low-lying states, we considered only the spontaneous decay. In Rydberg gases, the spontaneous decay is not the only loss channel of the system, but transfer of atoms induced by the black body radiation of a room temperature environment to the neighboring Rydberg states can be just as important.

As a matter of fact we know that the energy spacing between Rydberg levels scales as n^{-3} and, as example, we evaluated in Chapter 1 that the 70S state is roughly 23 GHz apart from the 71S state. In terms of λ it is ~ 13 mm. At such wavelength, photons from the black body radiation of a room temperature environment can couple the original Rydberg state to other Rydberg states, that are closely spaced in energy. As a consequence given enough time the content of the original Rydberg state will be spread over a number of different Rydberg states, with angular momentum $\ell' = \ell \pm 1$, each with its own properties.

The lifetime of the Rydberg level is thus dominated by two loss rates: spontaneous emission rate (Γ_0) and the rate of BBR induced transitions (Γ_{BBR}).

$$\Gamma_{eff} = \Gamma_0 + \Gamma_{BBR} \quad (3.1)$$

The first approach to calculate Γ_{BBR} comes from Cooke and Gallagher [19]. Who express the rate of BBR-induced transition $W(n\ell \rightarrow n'\ell')$ as the product of the Einstein coefficient for the spontaneous emission $A(n\ell \rightarrow n'\ell')$ and the number of photons at frequency ω from the black body distribution n_ω .

The coefficient of spontaneous emission $A(n\ell \rightarrow n'\ell')$ is proportional to the difference between the energy of the levels. As we saw in Chapter 1 such difference in Rydberg atoms can be expressed from the hydrogen-like description, in terms of the effective quantum number $n^{eff} = n - \delta_{n,j,l}$ and of the energy $E_{n\ell} = -1/(2n^{eff})^2$ of the n -th level. To simplify the notation we introduce $\omega_{nn'} = |E_{n\ell} - E_{n'\ell'}|$. So that we can write $A(n\ell \rightarrow n'\ell')$ as:

$$A(n\ell \rightarrow n'\ell') = \frac{4\omega_{nn'}^3}{3c^3} \frac{\ell_{max}}{2\ell + 1} R^2(n\ell \rightarrow n'\ell') \quad (3.2)$$

where ℓ_{max} is the largest of ℓ and ℓ' , $R(n\ell \rightarrow n'\ell')$ is a radial matrix element of the electric dipole transition.

The effective number of BBR photons is evaluated from the Plank distribution for the temperature T is:

$$\bar{n}_\omega = \frac{1}{e^{\omega_{nn'}/kT} - 1} \quad (3.3)$$

where k is the Boltzmann constant.

The total loss rate of the single state, due to the BBR-induced transfers is obtained taking into account all possible transitions to lower and upper states:

$$\Gamma_{BBR} = \sum_{n'} A(n\ell \rightarrow n'\ell') \frac{1}{e^{(\omega_{nn'}/kT)} - 1} \quad (3.4)$$

All the variables used in Γ_{BBR} are well known with the exception of the radial matrix elements $R^2(n\ell \rightarrow n'\ell')$ for the dipole transition, contained in $A(n\ell \rightarrow n'\ell')$.

Calculation of $R^2(n\ell \rightarrow n'\ell')$ differentiates the few theoretical [19–22] approaches to the problem. In this thesis we will follow the quasi-classical semi-empirical method developed by I.Beterov [22].

In [22] the dipole elements in Eq.3.4 are described in terms of harmonic oscillator. By introducing the oscillator strength

$$f(n\ell \rightarrow n'\ell') = \frac{2}{3}\omega_{n'n}R^2(n\ell \rightarrow n'\ell'). \quad (3.5)$$

we have:

$$\Gamma_{BBR} = \frac{2}{c^3} \sum_{n'} \omega_{nn'} |f(n\ell \rightarrow n'\ell')| \left[\frac{\omega_{nn'}}{e^{(\omega_{nn'}/kT)} - 1} \right] \quad (3.6)$$

The formula can be manipulated as follows:

1. The term in the square bracket varies slowly for $n > 15$ and can be brought out of the sum
2. Using the scaling laws of Rydberg atoms we can replace $\omega_{nn'} = 1/n_{eff}^3$.
3. The remaining sum over the oscillator strength satisfy the sum rule [23]

$$\sum_{n'} \omega_{nn'} |f(nL \rightarrow n'L')| = \frac{2}{3n_{eff}^2} \quad (3.7)$$

As a result, by applying the three changes described above, we obtain:

$$\Gamma_{BBR} = \frac{4}{3n_{eff}^5 c^3} \frac{1}{\exp(1/n_{eff}^3 kT) - 1} = \frac{1}{n_{eff}^5} \frac{2.14 \times 10^{10}}{\exp(315780/n_{eff}^3 T) - 1} (s^{-1}) \quad (3.8)$$

In order to improve the agreement of this calculation with numerical results the authors of the paper introduce four fitting parameters A , B , C , D , so that the final BBR induced transfer rate has the form:

$$\Gamma_{BBR} = \frac{A}{n_{eff}^D} \frac{2.14 \times 10^{10}}{\exp(315780B/n_{eff}^C T) - 1} (s^{-1}) \quad (3.9)$$

coefficients A, B, C, D changes for the element and with the angular momentum ℓ . For S-state in Rb they are $A = 0.134$, $B = 0.251$, $C = 2.567$, $D = 4.426$.

State	Experimental lifetime μs	Model lifetime μs	Reference (exp.value)
$30S_{1/2}$	14.5(12)	16.392	M.Mack [26]
$40S_{1/2}$	38()	36.254	T.Zhou [30]
$45S_{5/2}$	24.4(10)	49.154	D.B.Branden [31]

Table 3.1: Comparison between some of the experimental lifetimes measured in the literature [26, 30, 31] and those predicted by the model [22]

The total loss rate of the single state can be obtained substituting Γ_{BBR} in Eq.3.1.

The limit of validity of this approach is constituted by the ionization limit for which the interaction of the Rydberg electron with the BBR becomes comparable with the Coulomb interaction that binds it to the ionic core. This gives the relation

$$kT \sim \left(\frac{15}{32\pi^3} \right)^{1/4} \alpha^{5/4} \frac{m_e c^2}{n^2} \quad (3.10)$$

Where we used α for the fine-structure constant, m_e for the electron mass and c for the speed of light. From Eq.3.10 at room temperature (300K) we extract the maximum level of applicability $n=122$.

For Rydberg states with $30 \leq 50$ the model is in good agreement with experimental results, some examples for S-states are reported in Tab.3.1 For the 70S state, the one we use in the experiment, predicted lifetime is 151, 55 μs .

Chapter 4

De-excitation

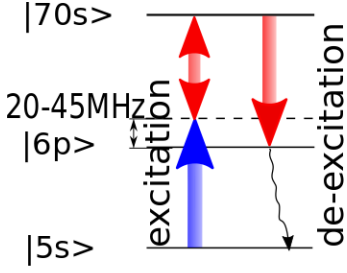
4.1 Introduction and experimental protocol

We now introduce a de-excitation technique that will be used in the following chapters to analyse many-body behavior and the deriving deviations from the two-level model due to BBR-induced state transfer. The main character of the de-excitation technique is to transfer excited atoms with a specific energy to the ground state. The transfer occurs thanks to a laser beam that couples the atoms with the target energy (that we will consider in state e) with a fast decaying state f , from where they decay spontaneously to the ground state g . The absence of a coupling from g to f makes it impossible for atoms in g to be re-excited to the original state e and consequently de-excitation is effectively a one-way transition from the Rydberg state to the ground state. The term 'fast' that defines f means that f should be empty at all times during de-excitation, otherwise atoms persisting in f can be excited to e by the laser radiation. Thus 'fast' refers not only to the dynamics of the effects we want to probe, but also to the characteristic timescales of de-excitation that will be introduced in the next sections.

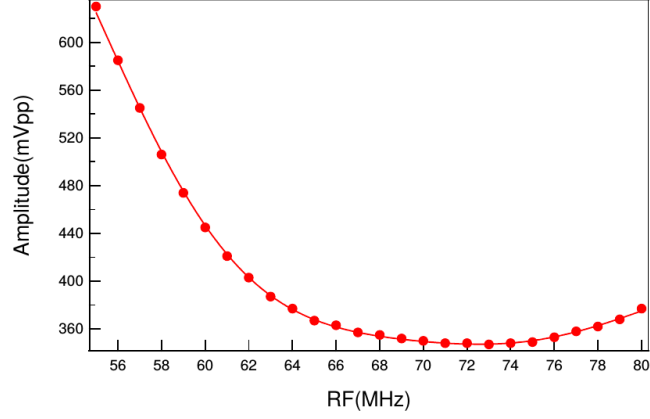
When the fast decaying state can be considered empty, de-excitation proves to be a highly sensitive and very versatile instrument; nevertheless up to now it has found only few applications either in combination with non-selective field ionization [24] or with different detection techniques [25, 26].

In Chapter 5 we will use the de-excitation technique in the investigation of many-body effects to probe the energy shifts induced by van der Waals interactions; while in Chapter 6 we will use the de-excitation technique in the investigation of multi-level effects to achieve state selectivity.

The basic protocol of de-excitation is similar for the two applications and will be de-



(a) The Rydberg sample is prepared exciting part of ground state atoms to the $70S$ state, in a two-photon process via a virtual level detuned by 20-45MHz with respect to the $6P_{3/2}$ state. De-excitation is resonant with the $70S \rightarrow 6P_{3/2}$ transition. The atoms in the $6P_{3/2}$ state decay at the fast rate $\Gamma = 7.9$ MHz. The absence of a coupling between ground and $6P$ prevents the atom from going back to $6P_{3/2}$ and makes de-excitation a one way process $70S \rightarrow 5S_{1/2}$



(b) In order to perform spectroscopy with the AOM, we need to compensate the change of the diffraction efficiency due to the RF. The curve shown correspond to ~ 12 mW, $\sim 20\%$ of the maximum power.

Figure 4.1: Excitation protocol

scribed in detail in this chapter so to provide the basis for both chapters.

Fig.4.1a shows the excitation scheme used to prepare the atoms in the initial Rydberg state and the de-excitation scheme implemented to probe such a state.

To prepare the Rydberg state, part of the atoms in the ground state are excited to the $70S$ state in a two-photon excitation scheme, via a virtual level slightly detuned with respect to $6P$ state, as explained in detail in 2.3. The excitation lasts τ_{exc} and at the end of the excitation, the beams are turned off.

The state is, then, interrogated through the de-excitation technique. That consists in the application of a laser pulse resonant with the $70S \rightarrow 6P$ transition, which lasts t_{dex} . The $6P$ state is the fast decaying state of our de-excitation protocol, with a decay rate to the ground state $\Gamma_{6P} = 7.9$ MHz.

The total number of Rydberg atoms remaining in the sample after de-excitation divided by the initial number of Rydberg atoms defines the de-excitation efficiency.

To generate the de-excitation pulse we use the same 1012 nm IR laser used for excitation

and we switch the frequency with an AOM (+1 order) in a double passage configuration (Sec.2.3). To be resonant with the two-photon transition during excitation and with the

$$70S \rightarrow 6P$$

the AOM must compensate the detuning of the lower transition laser δ_{6P} in the excitation, as shown in Fig.??.

Therefore, in our set-up, de-excitation limits the possible values taken by δ_{6P} to the range of efficiency of the AOM. To increase the range of possible detunings δ_{6P} , so as to allow to reduce the population of the 6P state as discussed in Sec.3.2.1, we want the AOM frequency range to be as wide as possible. However the diffraction efficiency of the AOM decreases for low RF frequencies, and, furthermore, depends on the angle between the beam and the RF propagation direction, as explained in Sec.2.3. We align the AOM to have the maximum diffraction efficiency of the +1 order around 73–75 MHz and we obtain a maximum power of ~ 70 mW, while we have ~ 12 mW for 55 MHz of the applied RF, which however is still sufficient for performing the experiment. Thanks to the double passage we are able to shift the frequency by up to 50 – 60 MHz

In the following we distinguish two kinds of de-excitation measurements: dynamics and spectroscopy. In the dynamics we probe the temporal evolution of the system over time by applying de-excitation pulses of different duration and with a constant frequency. In the spectroscopy we probe the energy distribution of the system, by applying pulses of the same duration, but different frequencies. The frequency variation is performed by changing the radio frequency applied to the AOM. To compensate the change in the diffraction efficiency of the device, we experimentally determine for each RF the amplitude that allows us to retrieve the same optical power after the double passage. We see an example of compensation curve in Fig4.1b. To obtain this curve we measure the output of the double passage configuration for a pulse of 50 μ s, for each frequency we change the amplitude of the RF-frequency, so as to obtain the same optical power. The curve reported allows us to keep an optical power ~ 12 mW, independently of the frequency.

In the investigation of many-body effects we will use both spectroscopy and dynamics to obtain complementary informations. In the study of multi-level effects we limit the investigation to dynamics.

4.2 Population of $6P_{3/2}$ and darktime

We now examine the characteristic timescales of de-excitation and demonstrate the validity of the 6P level as the fast decaying state of de-excitation. We start by considering the hypothesis that the 6P state may be populated at the beginning of the de-excitation pulse. In this case the de-excitation pulse can excite atoms from the $6P$ state to the $70S$ state. This process increases the number of Rydberg atoms and changes the initial state.

In Sec.3.2.1 we discussed the possibility to populate more hyperfine sub-levels of the $6P_{3/2}$ state. In that chapter we closed the discussion by using a positive detuning of the intermediate level from the upper hyperfine sublevel of the manifold. That expedient allowed us to neglect the hyperfine manifold, but we anticipated that population of the upper hyperfine sublevel $F = 3$ is still possible. We now reprise the topic and see how to circumvent the problem. We start by reporting the probability of the $5S \rightarrow 6P$ transition, that gives us the population of the 6P state. As we will work with low power of the 421 nm laser the probability is calculated in the first order perturbation theory with Fermi's Golden rule:

$$P_{g \rightarrow 6P} = \frac{1}{4} |D_{g,6p}(\Delta_{6p})|^2 I_{Blue} \tau_{blue} \quad (4.1)$$

where Δ_{6p} is the detuning of the 421 nm laser from the 6P level, I_{blue} the intensity of the blue laser, t_{blue} the pulse duration (that corresponds to the duration of excitation $\tau_{blue} = \tau_{exc}$) and $D_{g,6p}$ is the dipole matrix element for the transition $5s \rightarrow 6p$.

The parameters entering the $5S \rightarrow 6P$ transition probability are not free to set, but each of them has some constraint:

- The detuning Δ_{6p} is limited by the AOM efficiency range that is ~ 50 MHz.
- The duration of the pulse determines duration of the excitation; we want a narrow-band excitation, i.e we want the spectral width of the pulse to be within 10MHz, from the uncertainty principle we have $\tau_{blue} \geq 0.5 \mu s$.
- The intensity of the 421 nm laser is indirectly limited by the two photon process. If we change the intensity of the blue laser, the Rabi frequency of the two-photon process must be compensated with Ω_{IR} .

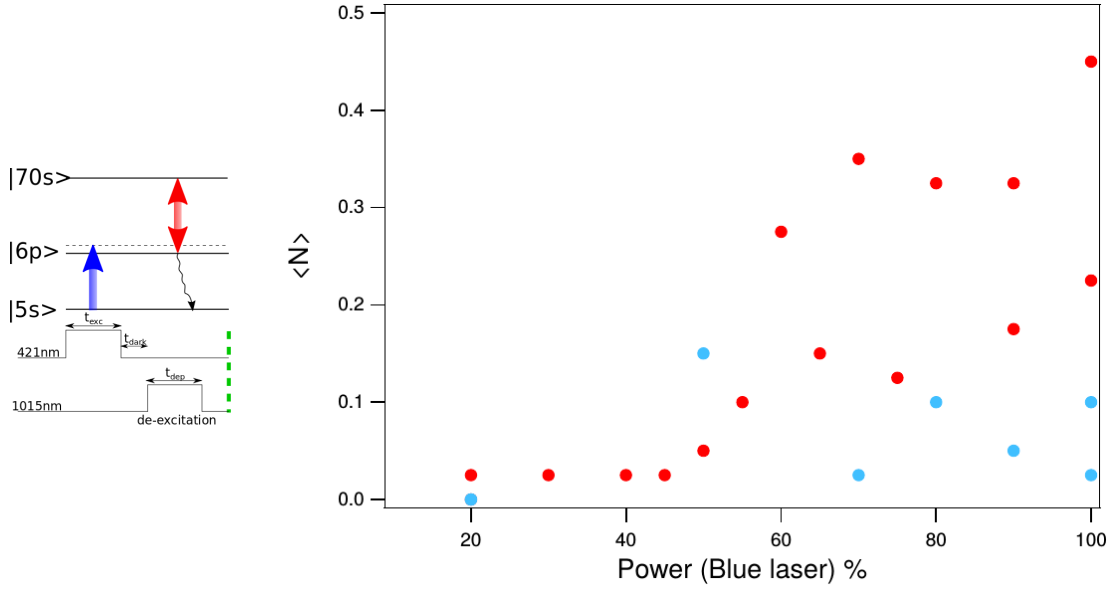


Figure 4.2: Rydberg atoms ($\langle N \rangle$) created from the residual population of the $6P$ state after $0.5 \mu s$ 421nm pulse. The IR pulse is turned on resonant with the $6P \rightarrow 70S$ after 300 ns (blue) or 500 ns (red) darktime from the end of the 421 nm pulse, to excite potential atoms in the $6P$ level to Rydberg state from where they can be detected. The x-axis reports the blue power as a percentage of 2.1 mW.

As final expedient we introduce a waiting time *darktime* between excitation and de-excitation. The darktime should be long enough to let atoms in the $6P$ level decay, but at the same time it should be short enough to makes possible to neglect in the meanwhile the thermal atomic motion, which we will see in Sec.1.4 changes the interaction energy.

We observed that the optimal duration of the darktime depends on the total population accumulated in the $6P$ level, hence on the parameters seen above; therefore it must be evaluated for each experiment. To do so we proceed as follows: first we apply the 421 nm pulse for the same time that it will be use for excitation, then we wait for darktime τ_{dark} and successively we apply a short pulse resonant with the $6P \rightarrow 70S$ transition to excite potential atoms in the $6P$ level. Finally we detect the Rydberg atoms right after the end of the de-excitation pulse.

An example of such measurement is shown in Fig.4.2 as a function of the power of 421nm laser for two different darktimes 300 ns and 500 ns. On the x-axis we report the power of the 421 nm laser as a percentage of 0.2 mW, for a pulse of duration $0.5 \mu s$. We

observe that for a darktime of 500 ns the number of Rydberg atoms detected is always below $\langle N \rangle = 0.15$, independently of the laser power. In a typical measurements with low number of Rydberg atoms $\langle N \rangle \sim 25$, the contribute from the population of the $6P$ level is less than 1% and we consider this fraction negligible. For $\tau_{dark} = 300$ ns the number of Rydberg atoms detected increases when the power of 421 nm laser exceeds 50%. In a typical measurement of $\langle N \rangle \sim 25$ such an increase in the number of Rydberg atoms due to the de-excitation pulse can be relevant to shift the system to different interacting configuration. In this case we would work below the 50% of the power. We observed that the typical duration of darktime is few times the mean lifetime of the $6P$ level.

4.3 Coherent dynamics, Rabi frequency and slowdown of de-excitation

Similarly to Sec.1.3, we introduce a coherent and incoherent regime for de-excitation. This means comparing the Rabi frequency driving the $70S \rightarrow 6P$ induced transition Ω_{dex} with a decoherence rate γ_{\perp} . In the de-excitation γ_{\perp} is dominated by the loss of atoms from the $6P$ level that has a rate $\Gamma_{6P} = 7.9$ MHz. Then the coherent regime is identified by the relation for $\Omega^2 \gg \gamma_{\perp}$.

This section briefly shows the effects of coherence, while in the following we will always consider a completely incoherent regime.

In the coherent regime the system undergoes damped Rabi oscillations. Fig.4.3 shows the dynamics for different Rabi frequencies of de-excitation: $\Omega_{dex} = 4 \times 2\pi$ MHz, $\Omega_{dex} = 2 \times 2\pi$ MHz, $\Omega_{dex} = 1.4 \times 2\pi$ MHz. The x-axis reports the de-excitation time, while the y-axis shows the number of Rydberg atoms normalized to its value before de-excitation. The grey area on the left of the plot represents the region in which the pulse area of the excitation pulse does not depend linearly on time due to the finite rise time ~ 60 ns of the AOM.

The experimental results have been compared with a damped oscillator [27] that includes losses from $6P$ and $70S$, respectively with rates Γ_{6P} and $\Gamma_{70S} = 1/\tau_{70S} \sim 7$ kHz¹ [22] The curves from the model have been shifted by 60ns to account for the AOM rise time. Although simple, this model(solid line in the figure) represents well the behavior of our system and it allows us to extract an effective Rabi frequency from the data.

On a longer timescale, reported in Fig.4.4 the oscillations are damped due to the transition decoherence introduced by the decay from the $6P$ level. We can observe that

¹This rate will be discussed in Chapter 6

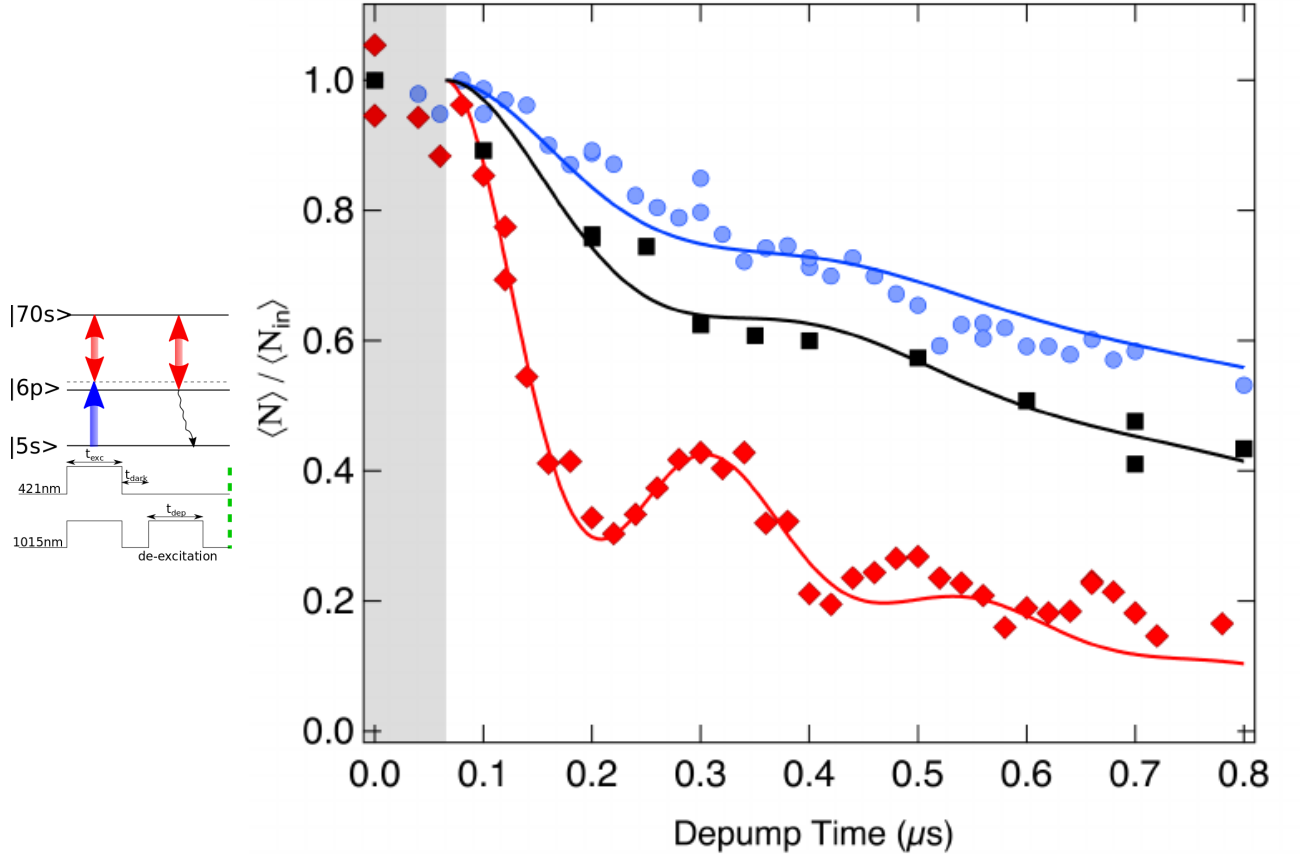


Figure 4.3: Rabi oscillation in de-excitation. The experimental points correspond red $\Omega_{dex} = 2\pi \times 4$ MHz, black $\Omega_{dex} = 2\pi \times 4$ MHz and green $\Omega_{dex} = 2\pi \times 4$ MHz. As the Rabi frequency decreases we approach the incoherent regime and oscillations are damped. Data agree with a coherent model of a damped oscillator (solid lines).

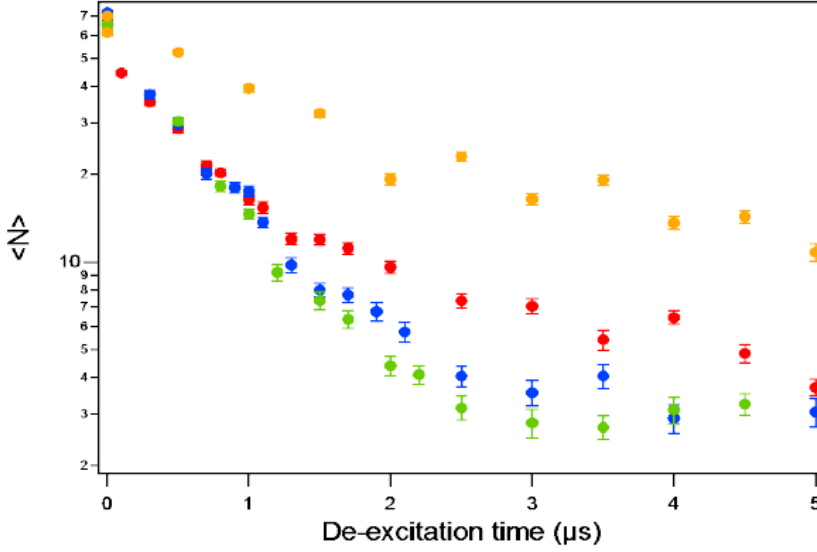


Figure 4.4: Residual Rydberg atoms $\langle N \rangle$ as a function of the de-excitation time for de-excitation Rabi frequency $\Omega_{dex} = 5.04 \times 2\pi$ MHz, blue $\Omega_{dex} = 3.56 \times 2\pi$ MHz, green $\Omega_{dex} = 2.78 \times 2\pi$ MHz, yellow $\Omega_{dex} = 0.91 \times 2\pi$ MHz. For $\Gamma_{6p} \leq \Omega_{dex}$.

for the lowest Rabi frequency of de-excitation $\Omega_{dex} = 0.91 \times 2\pi$ MHz the de-excitation rate is effectively smaller than for the three higher frequencies $\Omega_{dex} = 5.04 \times 2\pi$ MHz, $\Omega_{dex} = 3.56 \times 2\pi$ MHz, $\Omega_{dex} = 2.78 \times 2\pi$ MHz. The curves at the three higher frequencies seem to have a very similar decay rate in the initial part of the dynamics. This is to be expected as for those Rabi frequencies the de-excitation rate is limited by the decay rate of the 6P level.

We also observe that after the initial μ s the curves at the higher frequencies split, with the $\Omega_{dex} = 5.04 \times 2\pi$ MHz having a smaller de-excitation efficiency with respect to intermediate values of Ω , which does not agree with the simple picture just described. Further experiments are needed to identify the mechanism responsible for that behaviour.

4.4 Conclusion

We introduced a de-excitation technique, that transfer the atoms from the 70S state to the ground state through an optical coupling of the 70S with a fast decaying state 6P. De-excitation is a one way process only when the 6P state is empty at all time, therefore we examined the case in which the 6P state is populated during the excitation, which

leads to the introduction of a dark time. Also, we examined the case in which the 6P state is populated during the de-excitation, this case depends on the Rabi frequency of de-excitation and on the decay rate of the 6P state. Discussion of this case led to the introduction of coherent and incoherent de-excitation regime defined respectively as $\Gamma_{6p} \leq \Omega_{dex}$. $\Gamma_{6p} \gg \Omega_{dex}$. In the following de-excitation will be always used in the incoherent regime to perform dynamics and spectroscopy measurements.

Chapter 5

De-excitation as a probe of many-body effects

5.1 A simpler dynamics

We explained in Chapter 1 that in our experiment excitation of Rydberg atoms is a highly correlated process that involves all the ground state atoms in the effective volume. As a result the behavior of this system is difficult to predict: the large number of correlations discourages an analytical models, while the large number of variables exceeds computational possibilities.

De-excitation allows us to introduce a simpler dynamics on the system [28], in which:

- the initial sample is composed by Rydberg atoms that are typically up to ~ 60 , compared to $\sim 10^5$ atoms in the ground state that take part in the excitation dynamics.
- the transfer is one-way and the atoms are effectively removed from the initial sample, while the excitation can drive the transition from the ground to the excited state and vice versa

The simpler dynamics, as we will show, reveals additional information that is hidden in the complex dynamics of the excitation, and facilitates the computational analysis of the system.

To better understand the differences between excitation and de-excitation and the origin of the additional information provided by the de-excitation, we report the example of a small 1D chain, shown in Fig.5.1a, with atoms at distance $r_b/2$, where r_b is the

blockade radius introduced in Sec.2.3

During on-resonance excitation the atoms are initially created at a distance greater or equal to the blockade radius for which we consider the van der Waals interactions negligible. If we now want to excite one atom in an intermediate position, hence closer than r_b , the van der Waals interactions shift the Rydberg state of that atom out of resonance.

If successively we apply de-excitation to such a sample, we can de-excite all atoms that are further apart than r_b , hence non interacting in our approximation. However not only the last atom created will be off-resonant but also its neighbours. De-excitation of those atoms has, therefore a lower probability and slows down the dynamics.

Suppose now to start from a chain with all positions occupied, as can be created by off-resonance excitation. In this case all the atoms are interacting with their neighbours and there is no atom at resonance with the $70S \rightarrow 6P$ transition. By changing the de-excitation frequency to compensate for the shift due to van der Waals forces, we can select atoms in the chain with one or two nearest neighbours.

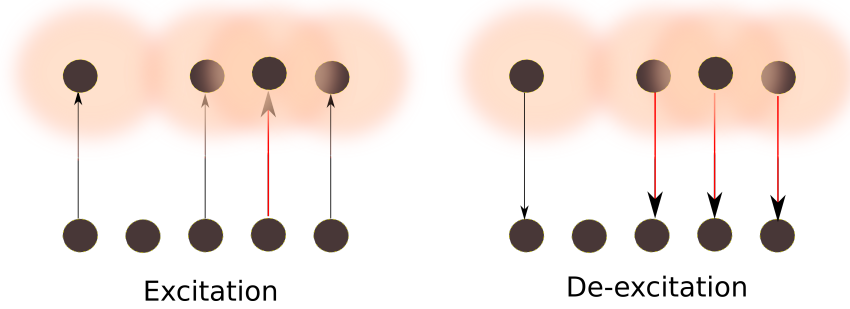
From a different perspective if we perform spectroscopy of an unknown 1D system we are able to probe the energy shifts due to the interactions, thus to extrapolate information on the spatial distribution of the excited atoms.

In the following we prepare the sample with resonant excitation to observe the cross-over between non-interacting and interacting regime, explained in the next section. Then we prepare the sample with off-resonant excitation to obtain a better control on the interactions and the spatial distribution of the sample and show a correspondence between the expected sample geometry and the de-excitation results.

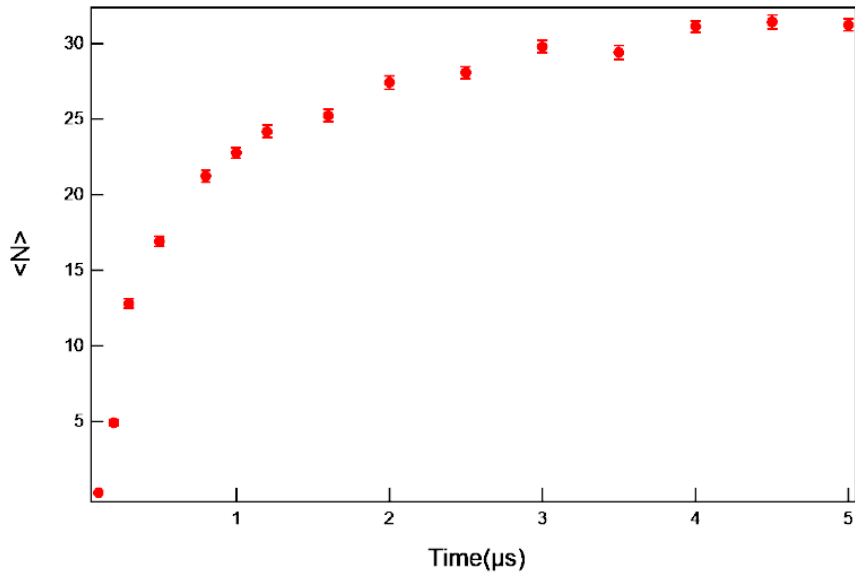
Data presented in this chapter refers to a quasi 1D geometry and are obtained for excitation and de-excitation in the incoherent regime as explained respectively in Sec.1.3 and in Sec.4.3.

5.2 On resonance excitation

We start by applying the de-excitation after resonant excitation, in a 1D geometry, similarly to the hypothetical example above. This will provide information on the cross-over between interacting and non-interacting regimes, explained in the following. In order to do so we recall the main principles of the on-resonance excitation. The excitation dynamics for resonant radiation presented in Fig.5.1b can be divided in two parts. Initially the resonant radiation excites the atoms further apart than the blockade



(a) Atoms at distance $r \geq r_b$ are excited resonantly. The atom in an intermediate position is shifted off-resonance by the van der Waals interactions, thus its excitation has a lower probability (represented with the red arrow) and longer timescale. When de-exciting such a state there will be only one atom at resonance, while the other three are in an interacting configuration, thus have lower de-excitation probability.



(b) Mean number of Rydberg atoms as a function of time. For low number of excitation ($\langle N \rangle < 30$) we see an almost linear behavior. When we approach fully blocked regime in our effective volume, interacting Rydberg atoms are excited, and the lower probability associated with that process leads to a slowing down of the dynamics.

Figure 5.1: Excitation and de-excitation dynamic

radius, the probability of exciting then is the same for all such atoms, and hence the number of excitations grows linearly with time. This is called the *non-interacting* regime, as we neglect the van der Waals interactions and suppose that all the excited atoms have the same energy. In Fig.5.1b this regime goes up to about 30 excitations. In the non-interacting regime de-excitation can be resonant for all the Rydberg atoms, that consequently are de-excited with the same probability. Then we can think of de-excitation as a constant loss rate for the system and we expect an exponential decay of the Rydberg population.

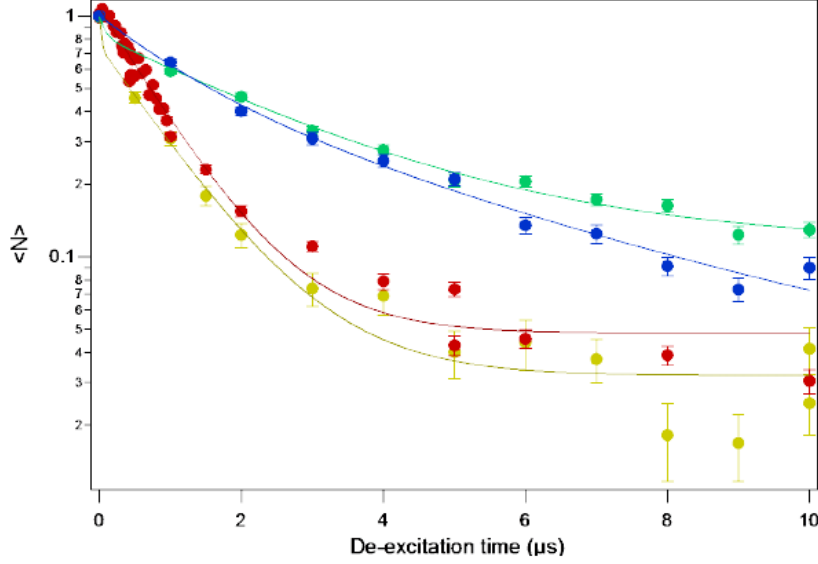
Now, if we increase the number of the Rydberg atoms in the system without changing the effective volume, some of the excitations will be created at distance $r < r_b$ in a region where the van der Waals interactions shift the energy. Due to the energy shift the radiation is not resonant with this transition, which thus has a lower probability. The decrease of the excitation probability slows down the excitation dynamics. This regime is called *interacting* regime. In this case we expect to de-excite resonantly only part of the atoms, as a matter of fact if we use a radiation resonant with $70S \rightarrow 6P$ transition as before, we are targeting only those atoms that are not interacting (and we expect to de-excite them with a rate similar to the previous). The expected dynamics for these atoms is in good agreement with an exponential decay. Similarly to the excitation dynamics, interacting atoms are not resonant with the de-excitation pulse and they determine a similar slow down in the de-excitation dynamics.

Combining the de-excitation dynamics on the interacting and non-interacting atoms of the interacting regime, we expect that de-excitation dynamics of the sample in the interacting regime is described by an overlap of two or more exponentials with different characteristic times due to the different energies of the atoms.

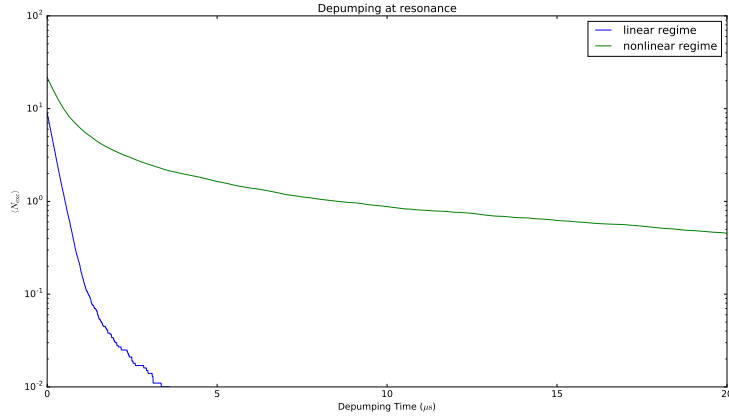
Fig.5.2a shows the de-excitation dynamics after resonant excitation for different initial number of excitations in the same volume in the interacting and non-interacting regime: $\langle N_i \rangle = 20$, $\langle N_i \rangle = 25$, $\langle N_i \rangle = 34$, and $\langle N_i \rangle = 45$. The excitation times used to obtain the different initial numbers range from $0.5 \mu\text{s}$ to $5 \mu\text{s}$, while the Rabi frequency of the processes is kept constant at $\Omega_{ex} = 1 \text{ MHz}$ for excitation and $\Omega_{dex} = 2.4 \times 2\pi \text{ MHz}$ for de-excitation.

The semi-log plot clearly shows a good overlap of all the curves in the initial part accordingly with the hypothesis that we are de-exciting non interacting atoms. Around $1 \mu\text{s}$ the curves taken for high initial numbers change rate and show the slow down of the de-excitation dynamics in the presence of interactions. This measurement confirms the sensitivity of de-excitation to interactions.

The experimental results have been compared with numerical simulations performed



(a) De-excitation dynamics after resonant excitation for $\langle N_i \rangle = 20$ (yellow), $\langle N_i \rangle = 25$ (red), $\langle N_i \rangle = 34$ (blue), $\langle N_i \rangle = 45$ (green) initial excitations in the same volume, hence different mean distance. $\langle N_i \rangle = 20$ and $\langle N_i \rangle = 25$ are in the non-interacting regime and agree with a single exponential decay down to a few percent. $\langle N_i \rangle = 34$ and $\langle N_i \rangle = 45$ in the interacting regimes, have slower rates in the second part of the dynamics.



(b) Simulation of de-excitation after resonant excitation in the non-interacting and interacting regimes. In the non interacting regime we see that de-excitation follows an exponential dynamics, while in the interacting regime de-excitation of interacting atoms has a lower rate. Simulations start from initial numbers: $\langle N_i \rangle = 9$ (blue), $\langle N_i \rangle = 20$ (green), $\langle N_i \rangle = 24$ (red).

Figure 5.2: De-excitation dynamics after resonant excitation

by Guido Masella, see Fig.5.2b. The simulations compute excitation and de-excitation process on a sample of 300 ground state atoms. The 1D geometry is realized placing randomly the atoms in a 1D lattice within 0.4 step size from their respective positions on a regular lattice. In the simulations the excitation uses a Rabi frequency of 100 kHz with a linewidth of 0.7 MHz while the de-excitation has a Rabi frequency of 1 MHz with 0.7 MHz linewidth and it drives transitions from the Rydberg state to the ground state. The two calculated curves in Fig.5.2b correspond to the non-interacting and interacting regime. In the non-interacting regime the de-excitation dynamics reproduces an exponential decay, while in the interacting regime there is a noticeable slow down of the de-excitation dynamics. These results reproduce qualitatively the same behavior observed in the experiment.

The loss of efficiency of de-excitation in the interacting regime can also be observed in spectroscopy. We prepare the initial sample as explained above. Then we apply a de-excitation pulse of $t_{dex} = 2 \mu s$, corresponding to the region in de-excitation dynamics in which the curves are well separated (see Fig.5.2a).

The results of de-excitation are shown in Fig.5.3a where we plot the mean number of Rydberg atoms as a function of the detuning of the de-excitation pulse from $|70S\rangle \rightarrow |6P\rangle$. We observe a resonant (anti-)peak whose amplitude decreases with the increase in the initial number of Rydberg atoms. This is in good agreement with the results of the excitation dynamics.

As we saw in the example in the previous section, the de-excitation spectroscopy provides also information on the spatial distribution of the atoms. In the case of resonant excitation we can wonder whether the atoms arrange in a self-ordered structure with a preferred distance among them. In that case the interaction energy would have a well defined value defined by the characteristic distances in the ordered structure; otherwise a disordered distribution of atoms would give rise to a disorder in the energy distribution.

In Fig.5.3a the absence of secondary peaks, other than the resonant one, suggests that there is no characteristic energy, corresponding to a characteristic distance.

Numerical simulations Fig.5.3b, run with the same parameters used for the dynamics, confirm the decrease of the peak amplitude with the increase of the initial numbers. In addition the simulations show an asymmetric broadening of the peak toward the blue side of the spectrum, with a long tail. The asymmetric broadening causes also a slight shift of the resonant frequency for increasing initial number of few hundredth kHz. These deformations are compatible with a wide distribution of interaction ener-

gies arising from a disordered spatial distribution of Rydberg atoms.

In the experiment we did not observe such deformations, a possible explanation can be due to the disorder in the radial direction present in the experiment, as opposed to the perfect 1D chains assumed in the theoretical model.

5.3 Off-resonant excitation

We now study the de-excitation spectroscopy and dynamics after an off-resonant excitation protocol, which as explained in Sec.1.4 provides a good control over the interaction energy. Off-resonant excitation in a quasi 1D geometry originates chains with regular spacing of atoms corresponding to the facilitation radius, up to saturation of the sample. The number of chains formed with off-resonant excitation depends on the probability of creating off-resonantly an isolated excitation that works as a spontaneous seed for the avalanche process; that probability on turn depends on the detuning Δ from the 70S state.

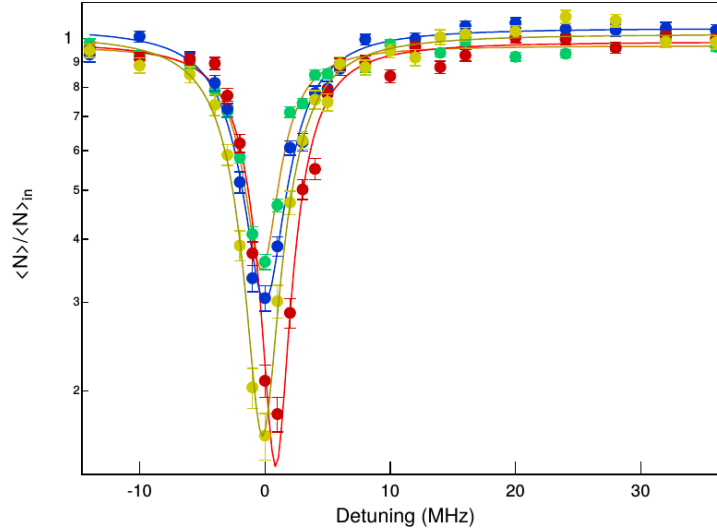
In the hypothesis of the creation of chains with a regular step-size the energy shifts due to van der Waals interactions are discrete, with just three possible values:

- $E = E_0$ for isolated atoms
- $E = E_0 + \Delta$ for atoms with just one nearest neighbour (extremes of a chain)
- $E = E_0 + 2\Delta$ for atoms with 2 nearest neighbours (middle part of a chain)

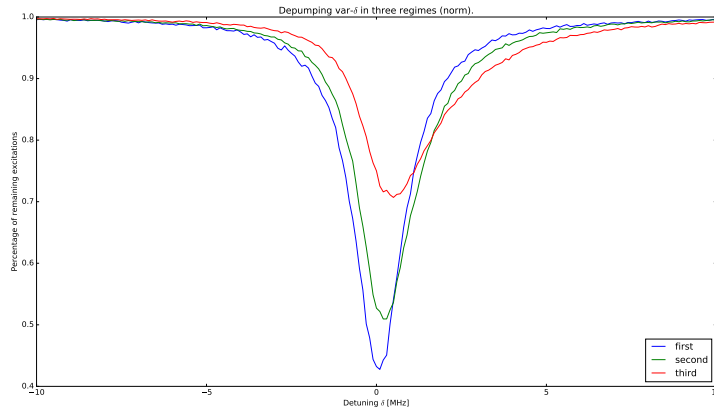
We want to realize such a system experimentally, but before doing it, we would like to discuss the role of the thermal motion in the interacting configuration, that will help the comprehension of the experimental parameters and of the variation of the experimental protocols.

We know that the atoms in the MOT have a temperature of $150 \mu\text{K}$ that corresponds to a mean thermal velocity of $120 \text{ nm}/\mu\text{s}$. During the experiment the MOT beams are turned off and the cloud expands under thermal motion. In this way the mean distance between the atoms increases, consequently the energy shift due to the van der Waals interaction decreases. At long evolution time, therefore, the interaction in the system will decrease.

The experimental protocol is as follows. The initial sample is prepared by applying an excitation pulse of $\tau_{dark} = 0.5 \mu\text{s}$, with detuning $\Delta_{exc} = +16 \text{ MHz}$ with respect to the 70S state, that corresponds to a facilitation radius of $8.82 \mu\text{m}$. The darktime is initially chosen as $\tau_{dark} = 0.5 \mu\text{s}$, so that during the darktime the atoms can move $\sim 60 \text{ nm}$ due



(a) De-excitation spectroscopy after resonant excitation. We observe a change in the amplitude of the de-excitation peaks. The curves are taken for $2\mu s$ de-excitation pulse and initial number $\langle N_i \rangle = 20$ (yellow), $\langle N_i \rangle = 25$ (red), $\langle N_i \rangle = 34$ (blue), and $\langle N_i \rangle = 45$ (green). Curves are normalized to the number of excitations before the de-excitation pulse. Solid lines to guide the eye are fits to Lorentzian curves.



(b) Numerical simulation of de-excitation spectroscopy for resonant excitation confirms the change in efficiency of de-excitation. The curves show also a slight deformation with a broadening of the peak and a shift toward higher frequencies. The curves are normalized to the number of excitation before de-excitation pulse: $\langle N_i \rangle = 9$ (blue), $\langle N_i \rangle = 20$ (green), $\langle N_i \rangle = 24$ (red).

Figure 5.3: De-excitation spectroscopy after resonant excitation

to the thermal motion. The energy shift due to the thermal expansion corresponds to a shift in frequency of 0.7 MHz, which is negligible in our system. De-excitation of this sample is shown in Fig.5.4. We found two different peaks at detuning $\delta_{dex} = 0$ and $\delta_{dex} = +16$ MHz from the $70S \rightarrow 6P$ transition, corresponding to E_0 and $E_0 + \Delta$. A third peak was expected around $\delta_{dex} = 32$ MHz corresponding to $E_0 + 2\Delta$; although we are not able to discern a peak in that region, we observe that de-excitation is still effective, this feature is compatible with the presence of atoms having that energy.

To confirm that the presence of the atoms with $E = E_0 + 2\Delta$ and the presence of the peak at $E = E_0 + \Delta$ are consequences of the interactions we increase the darktime of the measurement to give the atoms time to move further apart. The new darktime is chosen as $\tau_{dark} = 5 \mu s$, so that movement at mean thermal velocity is about $0.6 \mu m$. This distance is enough to shift by ~ 5 MHz the mean interaction energy of the atoms originally created at r_{fac} .

With this darktime we observe that the de-excitation efficiency decreases at $E_0 + 2\Delta$ and at $E_0 + \Delta$, but it increases at E_0 . The increase of the de-excitation efficiency at E_0 demonstrates a change in the energy distribution as expected for a spatial redistribution of the atoms due to the thermal motion. An even longer darktime would lead to a larger shift, but would also enter a time domain in which multilevel effects explained in Chapter 6 are not negligible, which is why we limited the darktime to $5 \mu s$ in this experiment.

The efficiency of the de-excitation at $E_0 + \Delta$ and $E_0 + 2\Delta$ appears even more striking if we compare the de-excitation dynamics for resonant and off-resonant excitation for the three frequencies E_0 , $E_0 + \Delta$ and $E_0 + 2\Delta$, as shown in Fig.5.5. On a qualitative level we see that de-excitation at E_0 is more efficient after resonant excitation, than after off-resonant excitation, accordingly to resonant excitation creating non interacting Rydberg atoms. On the contrary de-excitation at $E_0 + \Delta$ and $E_0 + 2\Delta$ is more efficient in the case of off-resonant excitation, which is compatible with the creation of the cluster.

5.4 Conclusion

We used the de-excitation technique to observe spectra and dynamics of quasi-1D samples of Rydberg atoms. The samples created through resonant excitation allowed us to probe the cross-over between interacting and non interacting regime, while the samples created with off-resonant excitation revealed how de-excitation can be used to indirectly observe the atomic motion. By comparing de-excitation measurements on the samples

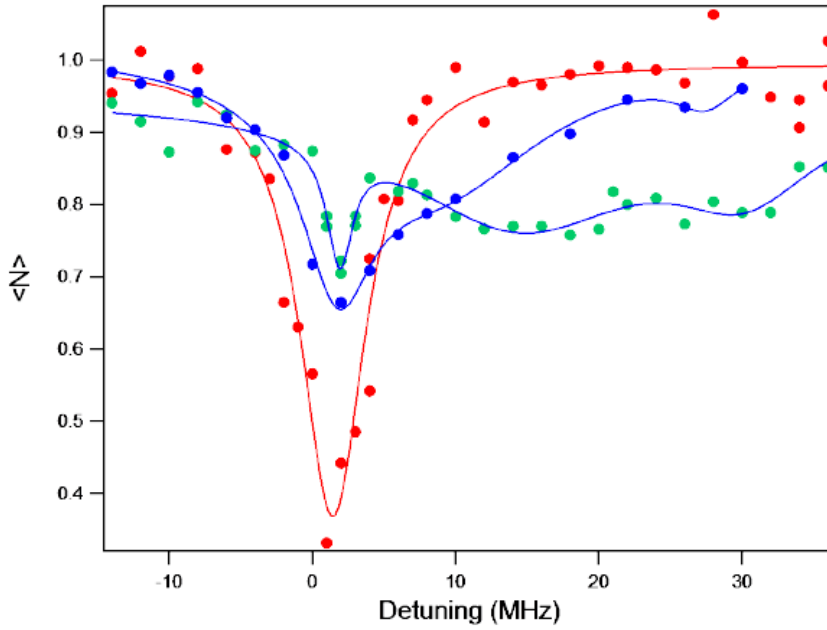


Figure 5.4: The red curve shows de-excitation spectroscopy after resonant excitation and is compared with de-excitation spectroscopy (green) after off-resonant excitation ($\Delta = 16$ MHz) and short darktime $0.5\mu s$. The comparison clearly shows that in the case of off-resonant excitation the presence of two peaks centered respectively at zero and Δ and a non-negligible de-excitation efficiency at 2Δ . Off-resonant excitation and a longer darktime (blue) corresponding to $5\mu s$. The second peak in the off-resonant excitation, due to interactions, disappears in blue curve as the atoms moves further apart. To guide the eye we fit a Lorentzian (three Lorentzians) on the spectra after resonant (off-resonant) excitation.

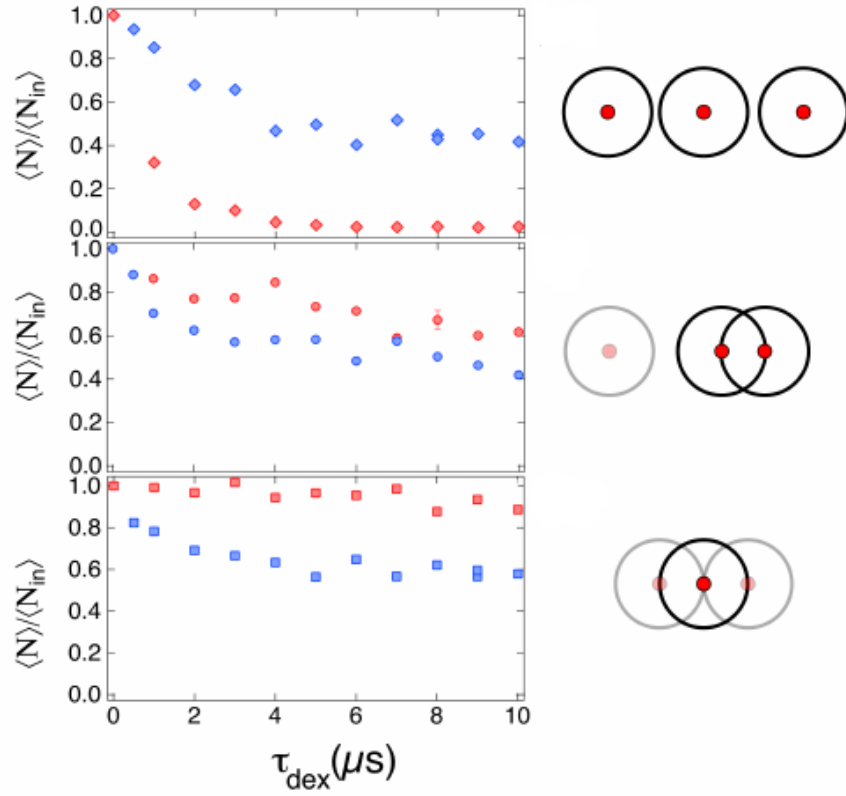


Figure 5.5: The red curves show the de-excitation dynamics after resonant excitation, blue ones the de-excitation dynamics after off-resonant excitation for the three frequencies from top to bottom E_0 , $E_0 + \Delta$, $E_0 + 2\Delta$. De-excitation at $E_0 + \Delta$, $E_0 + 2\Delta$ is more efficient after off-resonant excitation, compatible with the presence of atoms at that specific energy inside the cluster.

created with the two techniques we obtain information on the spatial configuration of the samples, such as the presence of long chains and that of isolated Rydberg atoms.

Chapter 6

De-excitation as probe of multi-level effects

6.1 Long dynamics and MOT decay

In the previous Chapter we discussed the many-body effects arising in the sample and to facilitate the interpretation of the results we approximated the system as a two level system with a ground state and an excited state and observed how the Rydberg state was modified by manybody effects. To be able to apply this approximation we limited the study of the dynamics within the initial $15 \mu\text{s}$, as for longer timescales state transfer mechanisms play an important role. In this chapter we use de-excitation to show how that time limit arises and how to measure the lifetime of the level.

The state transfer mechanisms modify the lifetime of the Rydberg state, as explained in Sec.3.2 Rydberg atoms have two main decay channels: spontaneous decay, which leads mainly to low energy states, and black body radiation induced transfers, which lead mainly to nearby Rydberg states. Although there are several theoretical [19–22] and experimental [26, 29–31] works on the topic, they regards mainly low Rydberg states from $n = 20$ to $n = 50$, in S, P or D state. Here we aim to measure the lifetime of the 70S Rydberg state. As indicative value for 70S lifetime we use $\tau_{70s} = 151 \mu\text{s}$ obtained in [22] with a semi-empirical method as we discussed in Sec.3.2. Consequently we probe the population of 70S state and the system dynamics over the interval from few μs to $\sim 1 \text{ ms}$. This time compared with previous experiments showed in this thesis is considerably longer and before discussing the measurement itself, we take a moment to discuss other mechanisms that could affect the number of Rydberg excitation measured over such a long timescale.

Typically the beams of the MOT, responsible for laser cooling, are turned off during the experiment to prevent the population of the 5P level and the artificial introduction of an additional level in the dynamics.

Without the beams the MOT is free to fall under gravity and to expand due to thermal motion, so that the number of atoms inside the effective volume changes. Let us suppose that initially the laser beams cross the MOT exactly in the center and that the MOT has a gaussian density profile for the three directions, so that we define the dimensions of the MOT along an axis as the variance of the gaussians along the same axis. We start by considering only the effect of the gravity which causes the MOT to fall by $\sim 10 \mu\text{m}$ over the first μs . Compared with the typical MOT diameter of $150 \mu\text{m}$, this distance can be considered negligible. Next we consider the expansion of the MOT due to the thermal motion of the atoms.

For each direction of space, the thermal motion leads to an expansion of the kind:

$$\sigma_i(t) = \sqrt{\sigma_i(0)^2 + (\alpha \langle v \rangle t)^2} \quad (6.1)$$

where α is a diffusion coefficient that we put arbitrary equal to one and v is the thermal velocity. From equipartition theorem the thermal velocity is:

$$\langle v \rangle = \sqrt{\frac{1}{2} \frac{kT}{m}} \sim 120 \text{ nm}/\mu\text{s} \quad (6.2)$$

where T is the cooling temperature $150 \mu\text{m}$ and m the mass of rubidium $\sim 1.7 \times 10^{-23} \text{ g}$.

To deduce experimentally the MOT expansion and fall, we measured the number of Rydberg atoms obtained from the same excitation protocol at different times after the shut down of the MOT beams. As the MOT expands isotropically its density decreases. The effective number of atoms in the effective volume can be obtained by integrating the density in the three directions: as the beams are copropagating the integral along the x axis extend on the interval $[-\infty, -\infty]$ and consequently is not affected by the MOT expansion in that direction. The integral on the radial direction is performed on the radial dimension of the effective volume (twice the smaller of the waist of the copropagating beams). The number of ground state atoms in the effective volume thus decreases as the expansion of the MOT in the radial direction.

The number of Rydberg atoms obtained with the same excitation protocol in the non interacting regime is proportional to the number of ground state atoms. In the approx-

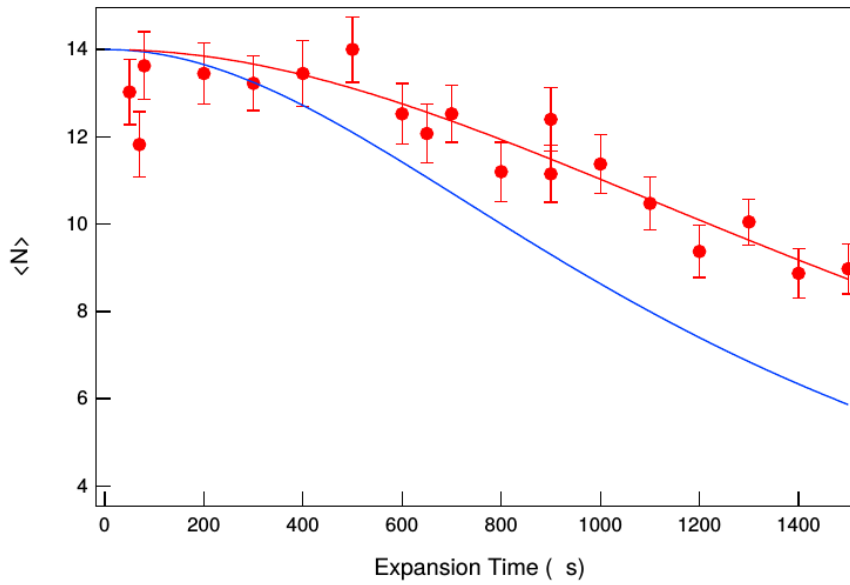


Figure 6.1: The expansion of the MOT leads to a decrease in the density of the atoms in the effective volume and consequently to a decrease of Rydberg atoms $\langle N \rangle$ created with the same excitation protocol at different times after the MOT beams are turned off. In blue the results of the model 6.3 for $\langle v \rangle = 120 \text{ nm}/\mu\text{s}$, in red the fit of the model to the data $\langle v \rangle = 79 \text{ nm}/\mu\text{s}$. We observe that effects of the expansion are negligible over the initial 1 ms ($\lesssim 15\%$).

imation that the density of ground state atoms is homogeneous in the effective volume the number of Rydberg atoms at a time t of the MOT expansion can be expressed as an easy function of the MOT dimension σ_i

$$N_{Ryd}(t) \simeq \frac{\sigma_y(0)\sigma_z(0)}{\sigma_y(t)\sigma_z(t)} N_{Ryd}(0) = \frac{\sigma_y(0)\sigma_z(0)}{\sqrt{\sigma_y(0)^2 + (\langle v \rangle t)^2} \sqrt{\sigma_z(0)^2 + (\langle v \rangle t)^2}} N_{Ryd}(0) \quad (6.3)$$

Experimental data are shown in picture 6.1. We choose an excitation time such that we obtain $\langle N \rangle \sim 5$ Rydberg atoms detected in a quasi 1D configuration, then we vary the time between the switching off of the beams and the beginning of excitation.

The measurements are performed on a MOT of 1 150 000 atoms, with $\sigma_z = 133 \mu\text{m}$, $\sigma_x = 241 \mu\text{m}$, $\sigma_y = 179 \mu\text{m}$. The data show that the total number of Rydberg atoms, hence of the ground state atoms in the effective volume decrease by $\sim 15\%$ over the initial ms. We consider this loss acceptable. The model is reported in blue in the image for a thermal velocity of $120 \text{ nm}/\mu\text{s}$ correspondin to a temperature of $150 \mu\text{K}$ proposed overestimates the loss of atoms. For completeness we report in red a fit of the model to the data with the mean thermal velocity as a free parameter that gives a thermal speed of $78 \text{ nm}/\mu\text{s}$ corresponding to $63 \mu\text{K}$. Due to the approximations done in the model, we consider this a good agreement. Thus additional effects that can change the number of atoms in the effective volume, such an asynchrony in the turning down of the beams, are by comparison neglected. In the following we will suppose that the motion of the Rydberg atoms, even in the presence of the van der Waals interactions, is dominated by the thermal motion. Then for the experiments we fix the beginning of the excitation after $5 \mu\text{s}$ from the shut down of the beams and typically detect atoms within the first ms.

6.2 70s and support lifetime

We start by discussing the lifetime of the 70S state and we will see that the range of validity of the two-level model follows from the same measurement.

For this chapter we introduce a protocol based on de-excitation similar the one described in Chapter 4, but with a variable darktime. During the darktime we expect the atoms to be transferred out of the Rydberg state:

- to neighboring Rydberg states, by BBR-induced transfer,
- to the ground state and to low excited states, by spontaneous decay

Due to the transfer, as the darktime increases the population of the 70S state decreases and we observe that de-excitation removes less and less atoms from the sample.

We probe the dynamics of the system as a function of the darktime. For each time we measure the total number of Rydberg atoms with $n \gtrsim 40$ (determined by the maximum electric field we can apply for field ionization) that we will call the *support* and that includes atoms in the 70S state. Then we introduce a short de-excitation pulse that removes $\geq 90\%$ of the atoms in the 70S state just before detection. Finally we measure the residual Rydberg population.

The duration of the de-excitation pulse is $\tau_{dex} \sim 5 - 10 \mu s$ and thus negligible if compared to the $100 - 1000 \mu s$ timescale over which we monitor the evolution of the system. Schematization of the protocol is reported in Fig.6.2.

The difference between the support and the residue after de-excitation is taken as the population of the 70S state. In the experiment the curves are taken in parallel, alternating the points as to exclude drifts and longterm fluctuations of the experimental apparatus.

A typical experimental result is shown in Fig.6.2. Here we use $5 \mu s$ de-excitation pulse, with a de-excitation efficiency of 95% calculated at low number and $\tau_{dark} = 0.5 \mu s$. The green data refer to the support and have a decay time of $344 \mu s$. The blue data are for de-excitation pulse before the detection, hence after removal of 70S and finally the red ones are the difference of the first two sets of data, representing the population of the 70S state.

First of all from the inset of 6.2 we see that 10% of the atoms are transferred out of the initial state, within $\tau_{dark} \sim 15 \mu s$. We take this as a threshold for the influence of multi-level effects on the system, thus it justifies the limit to the dynamics imposed in the previous chapter.

The population of the 70S state decays exponentially with a characteristic time $\tau_{70S}^{(meas)} \sim 80 \mu s$. This value differs by almost a factor two from the expected lifetime of the 70S state $\tau_{70S}^{(exp)} = 151 \mu s$.

We want to evaluate if this discrepancy can be due to interactions. To do so, we repeat the measurement and increase the initial number via the power of 421nm laser so as to reach the interacting regime in the initial sample.

To distinguish the effect of the interactions, from a possible dependence on the number we use also different interaction conditions. Initially we work in a small MOT in the quasi-1D configuration, so that atoms have two nearest neighbours. The small MOT has 288 000 atoms and diameters for the three directions $\sigma_x = 143 \mu m$, $\sigma_z = 72 \mu m$ and $\sigma_y = 101 \mu m$. The effective volume is $V_{1D}^{(sm)} \sim 30\,000 \mu m^3$. Then we switch to a big

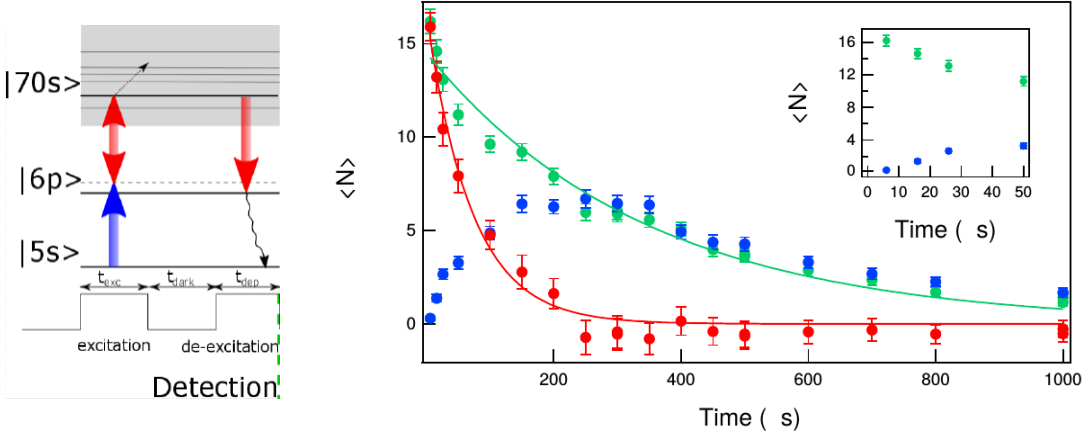


Figure 6.2: Example of a lifetime measurement. We change the dark-time and detect the Rydberg population without de-excitation pulse, called the support (green), and with a short de-excitation pulse (blue). The red points are the difference of the two sets of data and represent in our assumptions the population of the 70S state. The exponential decay of red points reflects the lifetime of the 70s state $\tau_{70S} \sim 80 \mu\text{s}$.

MOT and 3D configuration, so that atoms have 6 nearest neighbours. The big MOT has 1 684 000 atoms and measures $\sigma_x = 265 \mu\text{m}$, $\sigma_y = 200 \mu\text{m}$ and $151\sigma_z = \mu\text{m}$, so it has an effective volume of $V_{3D}^{(bg)} = 1\,300\,000 \mu\text{m}^3$. In the latter MOT 50 excitations distributed uniformly in the effective volume have a mean distance of $\bar{d}_{3D}^{(bg)} \sim 30 \mu\text{m}$, well above the blockade radius, while in the small MOT and 1D configuration 50 excitations are at a mean distance of $\bar{d}_{1D}^{(sm)} \sim 8.4 \mu\text{m} < r_b$, below the blockade radius, thus interacting.

Fig.6.3 shows the lifetime of the 70S state for the two geometries as a function of the initial number. Each point corresponds to a graphic similar to Fig.6.2 and represents the characteristic time of the exponential, the errors reported are the errors on the fits. We observe that all values are comparable within the error. Thus it seems that the lifetime of the 70S state does not depend on the initial interactions in the sample.

Fig.6.4 shows the variation of the lifetime of the support, evaluated from the single exponential fit shown in Fig.6.2. As above we changed the MOT dimension and the geometry of the system. Additionally we try to change the number both with the power of the 421 nm laser and with the excitation time. Theoretically the excitation probability depends on the product $\Omega^2 t$ and the two ways use to increase the initial number are equivalent, however in the experiment there are small differences: on one hand the

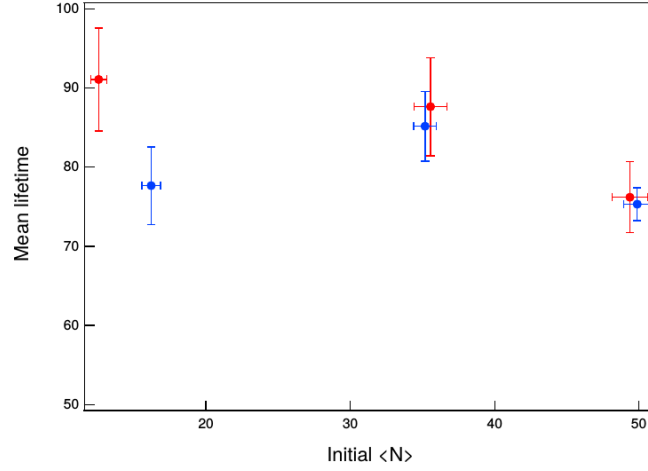


Figure 6.3: Lifetime of the 70S state measured as from Fig.6.2 across different interacting geometries: 3-dimensional effective volume in a big MOT(red), 1-dimensional effective volume for small MOT(blue). In each geometry the initial number is varied by changing the power of the 421 nm laser. The lifetime of the state does not seem to vary with the mean distance between the atoms, hence with the interactions.

atoms can move during excitation, so longer excitation time includes a rearrangement of the atoms; on the other hand, the increase of the power of 421 nm can induce power broadening in the transition and increase the disorder in the energy of the Rydberg atoms.

In all the cases of Fig.6.4 we observe that the mean lifetime increases with the increase of the initial number of Rydberg atoms and is considerably longer than the expected lifetime for S-P-D states close to the 70S state as seen in Tab.6.1. Furthermore we remark that the trend of lifetime is in quite good agreement for all configurations, suggesting that the lifetime depends on the total number of initial excitations rather than the mean distance between them and, hence, on the interaction energy.

6.3 Beyond 70S lifetime

We now broaden the multi-level picture analyzing what happens after the atoms leave the 70S state.

We know that the atoms leave the Rydberg state both from spontaneous decay or BBR radiation coupling, however BBR should be a symmetrical process so that atoms from nearby levels can be transferred back into the 70S state. To measure it we introduce a variation of the de-excitation technique.

n	S	P _{3/2}	D _{5/2}
55	83.151 μs	108.23 μs	87.226 μs
		110.40 μs	83.124 μs
60	103.53 μs	132.63 μs	107.92 μs
		134.87 μs	103.29 μs
65	126.32 μs	159.34 μs	131.05 μs
		161.85 μs	125.89 μs
70	151.55 μs	188.53 μs	156.63 μs
		191.30 μs	150.93 μs
75	179.25 μs	220.24 μs	184.69 μs
		223.27 μs	178.44 μs
80	209.42 μs	254.46 μs	208.93 μs
		258.17 μs	208.45 μs

Table 6.1: Single atom lifetimes of the Rydberg states from n=50 to n=80, as calculated in [22]

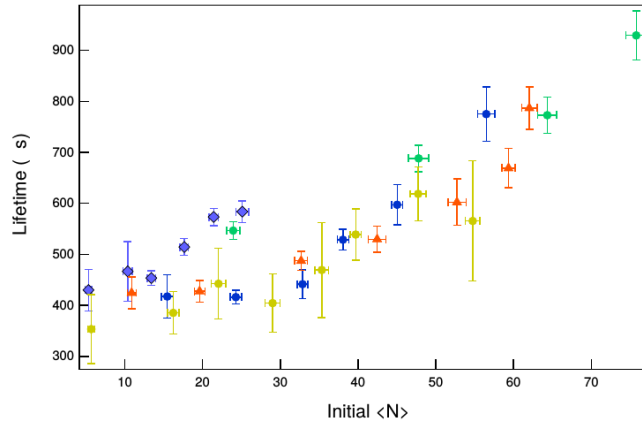


Figure 6.4: Lifetime of the support across different interacting regimes and geometries of the sample. In the green curve (3-dimensional effective volume in a small MOT), yellow (1-dimensional, big mot), blue (1-dimensional, small mot) the initial number has been changed increasing the power of the blue laser. For the orange curve (1-dimensional, small mot) the initial number have been changed with the excitation time. The violet curves corresponds to the lifetime of the support once the atoms in the 70S state have been removed. The lifetime of the support changes with the absolute number of Rydberg atoms in the initial sample, but does not seem to be influenced by the mean distance between them.

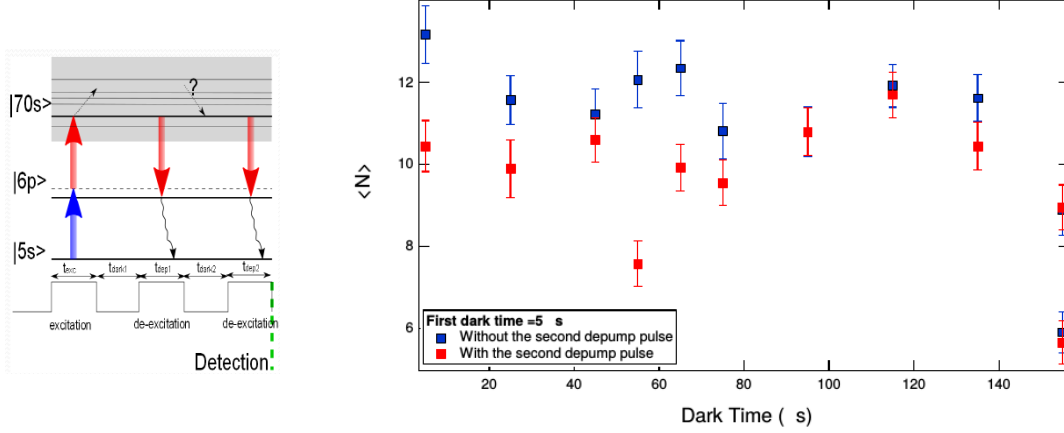


Figure 6.5: Experiment with two de-excitation pulses, separated by a variable darktime. We measure the value with (red) and without (blue) the second de-excitation pulse. The difference can be due to repopulation of the 70S level during τ_{dark2} or to residual population of the 70S state after the first de-excitation pulse.

We prepare the sample with $\tau_{exc} = 0.5 \mu\text{s}$ and let it evolve for $\tau_{dark1} = 10 \mu\text{s}$, so that the atoms are partially transferred out of the 70S state. Then we apply the de-excitation to the 70S state and empty the level within $t_{dex1} = 5 \mu\text{s}$. This is our initial state. From here we let the system evolve for a variable τ_{dark2} and finally we apply a second de-excitation pulse $\tau_{dex} = 5 \mu\text{s}$, right before detection. We measure the total number of Rydberg atoms with and without the second de-excitation pulse and observe the difference.

The results are shown in Fig.6.5. The curve taken with the second de-excitation pulse on seems to stay systematically below the one without the de-excitation pulse. This result confirms the presence of atoms in the 70S level at the moment of second de-excitation pulse.

On a qualitative level such a feature is compatible with the repopulation of the 70S state due to BBR-induced transfer, however we should use some caution and it will need a more thorough analysis on a quantitative level to distinguish repopulation from the residual population of the 70S state after the first de-excitation pulse.

We can also observe the dynamics of the system once we have removed atoms from the 70S state. We proceed as in the previous experiment and prepare the initial state by letting the system evolve for τ_{dark} after the excitation. Then unlike the previous experiment in which we turn off de-excitation and turn it on again in the end, we keep de-excitation pulse on at all time. In this way, atoms that are transferred back to the

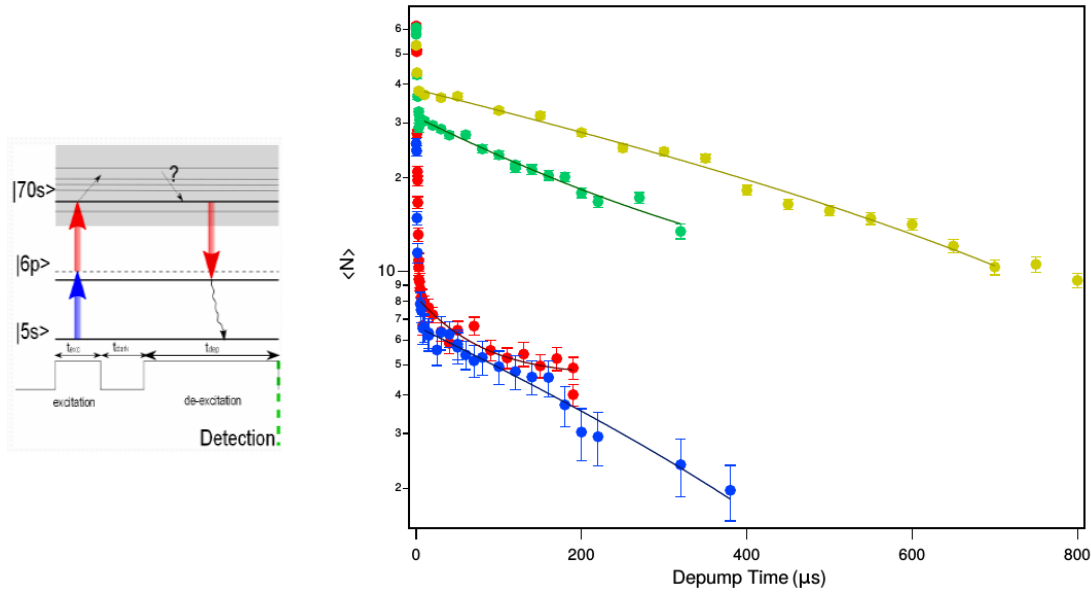


Figure 6.6: Dynamics with the de-excitation pulse constantly on, so that the atoms transferred back to 70s are immediately removed. The initial state is created with different darktimes: $0.5 \mu\text{s}$ (red circles), $10 \mu\text{s}$ (blue squares), $50 \mu\text{s}$ (green diamond) and $100 \mu\text{s}$ (yellow squares). The number of Rydberg atoms is reported on the y-axis, while the x-axis reports the time from the beginning of the de-excitation pulse. The solid lines are exponential fits to the second (slow) stage of the decay.

70S state are immediately removed from the system. We vary the duration of the de-excitation pulse and observe the total number of Rydberg atoms. The results of such measurement are shown in Fig.6.6. We observe that at short de-excitation time, the loss rate due to de-excitation is higher, corresponding to a steeper slope of the curve. This corresponds to the initial part of the dynamics where we remove atoms still in the 70S state. On longer timescales there is a second characteristic decay rate. After the original population of 70S has been depleted, keeping on the de-excitation pulse on at all time we look at the population of other Rydberg states. We observe that the second decay rate increases with increasing initial darktime. For increasing darktime the number of state different from the 70S state changes, hence it can be interesting to compare this result with the lifetime of the support in Fig.6.4. We expect that the second decay rate of these curves is shorter or similar to that of the support as the only difference is a dissipative process on one of the populated states. The result plotted in violet in Fig.6.4 is quite the opposite. As the darktime increases, thus the initial number of atoms transferred increases, the second decay rate of Fig.6.6 seems to grow

faster than the lifetime of the support. So far, we do not have a satisfactory explanation for this effect.

Furthermore we want to highlight that the lifetime of non-70S states measured here and the lifetime of the support measured in Sec.6.2 are longer than any level close to the 70S state. From the theory [22] we know that the lifetime of the single atom increases predominantly with the angular momentum of the state ℓ , but starting from S-state, the probability of reaching states with $\ell < 4$, by BBR transfer only is usually negligible [32].

6.4 Conclusion

The phenomenology observed in this chapter about the measured lifetime of the 70S state and the support is currently under investigation.

Here we want to discuss the discrepancy between the measured and the expected lifetime of the 70S state. To the best of our knowledge the 70S state is the highest level for which the lifetime has been measured so far, so we can only compare our measurements to experimental results on lower states reported in the literature ranging from 20 to 50, such as [25, 26, 30, 31].

A protocol like the one used here has been applied by M.Mack *et al.* [26] in combination with time resolved resonant absorption as detection technique, which reveals the Rydberg atoms as losses from the MOT. In the paper they measure the lifetime of the 30S and the 38D states and they find them in good agreement with the theory at room temperature (300K). The experimental conditions are similar to the one we used, with $\tau_{exc} = \tau_{dex} = 1 \mu s$ and Rydberg density $n_{Ryd} = 7 \times 10^9$. The good agreement between experiment and theory obtained in the paper seems to validate the protocol and pushes us to look for other effects beyond spontaneous decay and BBR induced transitions.

The lifetime of the 70S state we measured is about a half of what we expected. Such effect can be compatible with superradiant many-body effects [33] such as discussed in [25, 26, 30], although our experimental parameters are similar to those of [30] in which there was no evidence of superradiant effects. Further experiments and theoretical modelling will be necessary to explain our experimental results.

Conclusion

This thesis reports on the experimental investigation of many-body and multi-level effects in a cold Rb Rydberg gas. The aim of this thesis was to identify the range of validity of the two-level approximation and its limitations, and to develop a tool that allows us to clearly identify many-body and multi-level effects. This tool was found in a de-excitation technique, which permits us to detect with high sensitivity the small changes in the energy of the atoms and which induces a simpler dynamics on the sample. The technique has been realised with the introduction of a laser beam that couples excited atoms within a very narrow energy interval to a fast decaying state, specifically we used the 6P state which lies close to the virtual level of the excitation process. The simpler dynamics of de-excitation arises from the one-way nature of this transfer, which is fulfilled when the fast decaying state can be considered empty. In order to determine the range of validity of that assumption, we investigate the probability of populating this level either during the excitation or de-excitation processes and we found the range of parameters for which the population of the 6P state is negligible, such as detuning of the intermediate state of the excitation and darktime.

The use of the de-excitation technique in the investigation of many-body effects allowed us to probe the small changes due to the van der Waals interactions in the energy of the 70S state. We showed that those interactions among Rydberg atoms can split, broaden or shift the energy of the excited state by several MHz. De-excitation proved very sensitive to the cross-over between the interacting and non-interacting regime and, also, it allowed us to retrieve information on the spatial distribution of atoms in interacting samples.

The multi-level effects studied in this thesis derive from the population of the intermediate state of the excitation and from the transfers to the nearby Rydberg levels. The first case was probed with the excitation dynamics and showed the emergence of additional excitation pathways to the Rydberg state, that complicate the simple two-level picture. State transfer mechanisms leading to nearby Rydberg levels were probed

with the use of the de-excitation technique. We have used that technique to measure the lifetime of the 70S state in our experiment, in the light of all the potential state transfer mechanisms and decay channels, and we measured the lifetime of the total Rydberg population (support) in the energy states with $n \gtrsim 40$. We observed that the latter lifetime depends on the total initial number of atoms in the 70S state, but that changing the mean distance between the atoms, while keeping the number constant, does not seem to affect the lifetime. The lifetime of the 70S state, by contrast does not change the initial number of atoms in the sample, nor it does seem to change with the van der Waals forces. Furthermore the lifetime of the 70S state deduced from our measurements is shorter than that expected for just spontaneous decay and black body induced transfer.

From the measurements performed in this thesis we deduce that the two-level model can be applied only in the initial part of the dynamics, on a timescale on which the multi-level effects are negligible, which for our system corresponds only to the initials $15\mu s$. At the same time we observed that the excited state of the model is changed by the interactions.

To comment on this result we distinguish two cases: when the measurement requires fine probing of the interactions, the use of narrow band techniques in detection such as de-excitation [34], can be very useful. Instead, if the information on the effect is retrieved from the total number and such a fine distinction is not desired [35]. In the second case the application of narrow band technique requires a thorough characterization of the parameters.

The short lifetime measured for the 70S state opens many questions on the effective decay channels of high Rydberg states. Possible explanations of these results can involve single-atom or many-body effects such as super-radiance and require further investigation.

Appendix A

An example of repump laser

The experiment in which I worked in Stuttgart aims at the realization of Rydberg molecules, composed by an atom in the ground state and an atom in a Rydberg level. Such molecules were predicted by Fermi [36] and Greene [37] and observed experimentally for the first time in the 5th Physikalisches Institute of Stuttgart University [38], in a previous version of the experiment here referred. Since the first observation Rydberg molecules have been proposed as an effective instrument for the study of low-energy collisions [39] and chemical reactions [40]. The new experiment developing in the 5th Physikalisches Institute of Stuttgart University combines Rb and Li to study Rydberg heteronuclear molecules.

The main goal of the internship was the set-up of a repump laser for Rb.

The different purposes of Stuttgart's experiments shapes the experimental apparatus quite differently from the one used in Pisa although it maintains the same fundamental structure of all Rydberg atoms experiments: trapping, excitation, detection. In particular laser cooling, and therefore also the repump, of Rb works on the same transitions for the two experiments:

In order for the repump mechanism to work, it needs to selectively excite a well-defined hyperfine transition and hence, the linewidth of the laser must be smaller than the level separation. In the set-up we choose the linewidth of the laser to be $\lesssim 15\%$ of the smaller hyperfine separation, that is $\lesssim 10\text{MHz}$, as the linewidth of the $5P_{3/2}F \rightarrow 5P_{3/2}F = 1$, is 72MHz [41]. The chosen laser is a distributed feedback laser that has a nominal

Main Transition	$5S_{1/2}, F = 2 \rightarrow 5P_{3/2}, F = 3$
Off-resonant transition	$5S_{1/2}, F = 2 \rightarrow 5P_{3/2}, F' = 2$
Repump	$5S_{1/2}, F = 1 \rightarrow 5P_{3/2}, F' = 2$

linewidth of $< 10\text{MHz}$. As the linewidth is a critical value in the experiment we measure it before the set up with the delayed self-heterodyne technique [42].

This technique is a variation of the heterodyne technique common in both electronics and optics. In the heterodyne technique, the signal of two independent beams produces a signal whose spectral density is given by the convolution of the spectral density of the two beams, and which thus preserve the phase and frequency information of the two original beams.

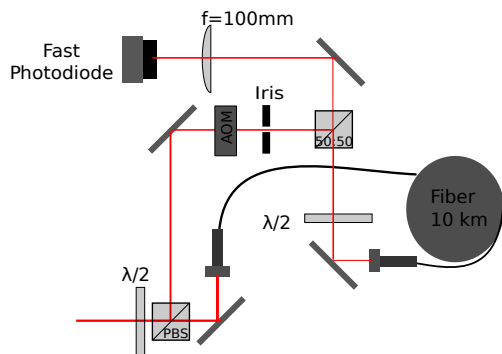
In delayed self-heterodyne technique, as we are about to see, we use just one beam in a Mach-Zehnder interferometry scheme and we made it interfere with an 'older' version of itself.

The laser linewidth arises from the presence of phase noise in the laser. Therefore, if the beam interfere with its 'current' self, the phase fluctuations in the two branches are correlated and they do not manifest in the interference signal. To be able to measure the linewidth of the laser, we need to remove the correlations in the phase fluctuations in the two branches. To do so we introduce a delay stage, so that the beam interferes with an older copy of its self. In this way the spectral components of the phase fluctuations faster than the delay are uncorrelated. A beam splitter overlaps the beams, the produced interference signal is observed on a amplified photodiode. The interference signal has a constant part and a beatnote. In the latter the fluctuations of phase are converted in fluctuation of the frequency, around a central frequency given by the difference in frequency of the two beams, which we provide by shifting one of the beams with an AOM (see Chapter 2). The spectrum of the beat note is then a Lorentzian with width equal to the $\sqrt{2}$ ×linewidth of the laser and the frequency equal to the frequency shift between the branches.

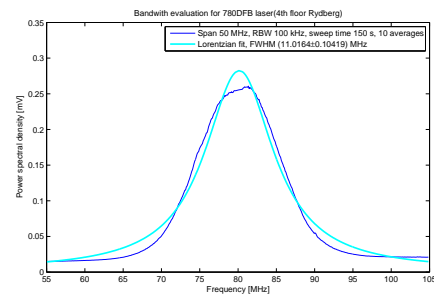
The experimental set-up for the self-heterodyne technique used to measure the linewidth of the DFB laser is shown schematically in Fig.A.1a We used a 10km fiber, that in the approximation that it is crossed at the speed of light in vacuum, induces a delay of $t_{del} \sim 3 \times 10^{-5}s$. Then only the spectral components of the phase fluctuation at frequency of order 100 kHz or slower remain correlated.

With this technique we measured a linewidth of 7.77MHz (Fig.A.1b), that is in good agreement with the nominal value of 10MHz and satisfies the demands of our application.

We now want to select a single transition and to operate durably the laser on resonance with it. Small fluctuations in the current or the temperature of the laser may induce



(a) Schematics of the self-heterodyne apparatus, with Mach Zehnder interferometry scheme. The beam is splitted in two branches with the aid of a polarizing beam splitter. One branch goes through a 10km fiber that acts as delay stage, so that correlations between the two branches are suppressed down to few hundred kHz scale at the exit of the fiber. The other branch is shifted in frequency of 80MHz. The two branches are overlapped with a beam splitter. The interference pattern is recorded with an amplified photodiode. The spectrum of the signal is a Lorentzian that has as center the frequency set on the AOM and as width the linewidth of the laser.



(b) Fourier transformation of the signal obtained with self-heterodyne technique. The center is at 80MHz, from AOM setting. The Lorentzian fit has a width of 11MHz. .

intensity is $I_{sat} \sim 3.57\text{W/cm}$. [41] In polarization spectroscopy the pump beam is above saturation intensity so that when this laser is on resonance with the atomic transition, the population of the ground state is reduced of more than 25% with respect to the total population, while the probe beam is below saturation intensity.

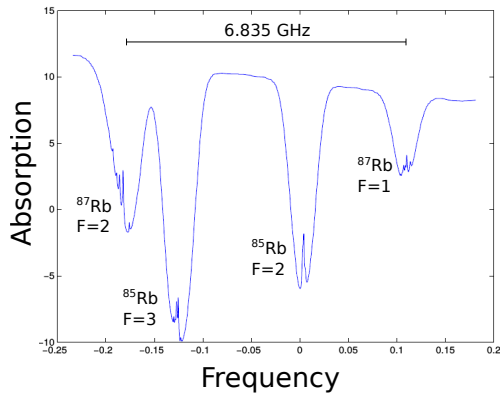
In the coordinate system of atoms at rest the pump and probe beams are at the same frequency. On resonance with the atomic transition the pump depletes partially the population of the lower state, so that absorption of the probe is reduced. In this conditions small holes, called lamb-dips, appear in the probe absorption spectra. On the contrary for atoms moving at $v \neq 0$, the beams are at different frequencies. Thus probe beam and pump beam will not be simultaneously on resonance with the atomic transition, and absorption of the probe beam is not modified by the presence of the pump beam. It follows that the width of the lamb-dips does not depend on the Doppler effects, but only on the laser linewidth [44]. This part of the technique is known also as saturation spectroscopy. Spectra from saturation spectroscopy has been observed as an intermediate step in the measurement. In Fig.A.3a we reported the so called D2-line of Rb, showing the $5S_{1/2}, F = 2 \rightarrow 5P_{3/2}$ and $S_{1/2}, F = 1 \rightarrow 5P_{3/2}$ of ^{87}Rb and the $5S_{1/2}, F = 2 \rightarrow 5P_{3/2}$ and $5S_{1/2}, F = 3 \rightarrow 5P_{3/2}$ of ^{85}Rb . In the picture are clearly visible the lambdips corresponding to the hyperfine transitions.

Polarization spectroscopy allows for even better defined signal. If we use a circularly polarized pump beam, it is possible to select the Zeeman sublevels of the $5P_{3/2}$ on which the laser acts. Depending on the sign of polarization either the level with the greater or lower m_F is depleted. That corresponds to lower or zeroing one spatial component of the F-momentum, hence it introduces an anisotropy in the medium.

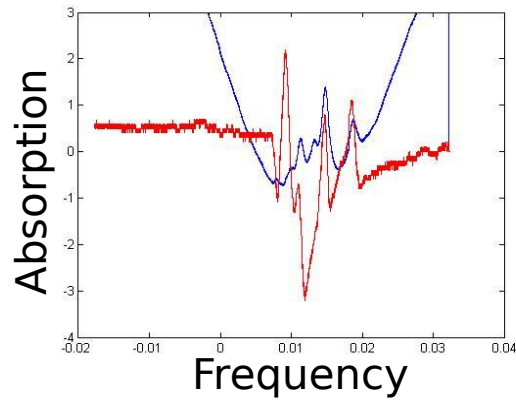
If the probe beam is linearly polarized when it crosses the medium, it experiences a birefringence, due to the presence of the pump, and the two axes of polarizations accumulate different delays. Splitting the probe beam after the cell with a polarizing beam splitter, it is possible to retrieve the two polarizations and observed this delay.

In Fig.A.3b we observe the spectrum of the $5S_{1/2}, F = 2 \rightarrow 5P_{3/2}$ transition and show the difference between saturation and polarization spectroscopy. Polarization spectroscopy signal has very steep ramps, with zero-crossings in correspondence of the hyperfine transitions. Hence we can use it as the error signal using the zero crossing as reference value, the steep variation around it provides high sensitivity to small frequency changes and permits a fast response through the feedback loop.

This signal was used as error signal to produce an electronic feedback on the current



(a) Spectrum of D2 line transition in ^{85}Rb and ^{87}Rb



(b) Spectrum of $|5S_{1/2}\rangle \rightarrow |5P_{1/2}\rangle$ line transition in ^{87}Rb

of the laser. The laser was tested in the laboratory at the current of 140mA that will be used in the experiment, that correspond to an optical power of 80mW. In this conditions the laser was stable over 24 hours.

Bibliography

- [1] P.W.Anderson, **More Is Different**, *Science* , 177, 393 (1972).
- [2] I.Bloch, J.Dalibard, S.Nascimb'ene, **Quantum simulations with ultracold quantum gases**, *Nature Physics*, 8, 267 (2012).
- [3] R.Feynman, **Simulating Physics with Computers**, *Int.J.Theor.Phys.*, 21, 467 (1982).
- [4] M.Saffman, T.G.Walker, **Quantum information with Rydberg atoms**, *Rev.Mod.Phys.*, 82, 2313 (2010).
- [5] J.Han, Y.Jamil, D.V.L.Norum, P.J.Tanner, T.F.Gallagher, **Rb n f quantum defects from millimeter-wave spectroscopy of cold 85 Rb Rydberg atoms**, *Phys.Rev.A*, 74, 054502 (2006).
- [6] T.F.Gallagher, *Rydberg Atoms*, Cambridge University Press (1994).
- [7] R.Löw, H.Weimer, J.Nipper, J.B.Balewski, B.Butscher, H.P.Büchler, T.Pfau, **An experimental and theoretical guide to strongly interacting Rydberg gases**, *J.Phys.B:At.Mol.Opt.Phys.*, 45, 113001 (2012).
- [8] D.Comparat, P.Pillet, **Dipole blockade in a cold Rydberg atomic sample**, *J.Opt.Soc.Am.B*, 27, A208 (2010).
- [9] I.Lesanovsky, J.P.Garrahan, **Kinetic constraints, hierarchical relaxation, and onset of glassiness in strongly interacting and dissipative Rydberg gases**, *Phys.Rev.Lett.*, 111, 215305 (2013).
- [10] J.Sanders, M.Jonckheere, S.Kokkelmans, **Sub-Poissonian Statistics of Jamming Limits in Ultracold Rydberg Gases**, *Phys.Rev.Lett.*, 115, 043002 (2015).

- [11] M.M.Valado, C.Simonelli, M.D.Hoogerland, I.Lesanovsky, J.P.Garrahan, E.Arimondo, D.Ciampini, O. Morsch, **Experimental observation of controllable kinetic constraints in a cold atomic gas**, *Phys.Rev.A*, 93, 040701(R) (2016).
- [12] R.Faoro, C.Simonelli, M.Archimi, G.Masella, M.M.Valado, E.Arimondo, R.Mannella, D.Ciampini, O.Morsch, **van der Waals explosion of cold Rydberg clusters**, *Phys.Rev.A*, 93, 030701(R) (2016).
- [13] C.Simonelli, M.M.Valado, G.Masella, L.Asteria, E.Arimondo, D.Ciampini, O.Morsch **Seeded excitation avalanches in off-resonantly driven Rydberg gases**, arXiv:1602.01257.
- [14] D.Ciampini, *Realization of a 87Rb Bose-Einstein Condensate: Atomic Physics with Coherent Matter Waves*, Ph.D. Thesis (2002).
- [15] F.Keffler, R.Loudon, **Simple Physical Theory of Spin Wave Interactions**, *J.Appl.Phys.* 32, S2 (1961).
- [16] M.Viteau, J.Radogostowicz, A.Chotia, M.G.Bason, N.Malossi, F.Fuso, D.Ciampini, O.Morsch, I.Ryabtsev, E.Arimondo, **Ion detection in the photoionization of a Rb bose-einstein condensate**, *J.Phys.B*, 43, 155301 (2010).
- [17] M.Viteau, J.Radogostowicz, M.G.Bason, N.Malossi, D.Ciampini, O.Morsch, E.Arimondo, **Rydberg spectroscopy of a Rb MOT in the presence of applied or ion created electric fields**, *Opt.Express.*, 19, 6007 (2011).
- [18] E.Courtade, M.Anderlini, D.Ciampini, J.H.Müller, O.Morsch, E.Arimondo, M.Aymar, E.J.Robinson, **Two-photon ionization of cold rubidium atoms with a near resonant intermediate state**, *J.Phys.B: At.Mol.opt.Phys.*, 37, 967 (2004).
- [19] W.E.Cooke, T.F.Gallagher, **Effects of blackbody radiation on highly excited atoms**, *Phys.Rev.A*, 21, 588 (1980).
- [20] C.E.Theodosiou, **Lifetimes of alkali-metal-atoms Rydberg states**, *Phys.Rev.A*, 30, 2881 (1984).
- [21] X.He, B.Li, A.Chen, C.Zhang, **Model-potential calculation of lifetimes of Rydberg states of alkali atoms**, *J.Phys.B* 23, 61990 (1990).

- [22] I.I.Beterov, I.I.Ryabtsev, D.B.Tretyakov, V.M.Entin, **Quasiclassical calculations of blackbody-radiation-induced depopulation rates and effective lifetimes of Rydberg nS, nP, and nD alkali-metal atoms with $n \leq 80$** , *Phys.Rev.A*, 79, 052505 (2009)
- [23] H.A.Bethe, E.E.Salpeter, *Quantum Mechanics of One- and Two-Electron Atoms*, Springer, Berlin (1957).
- [24] M.Mudrich, N.Zahzam, T.Vogt, D.Comparat, P.Pillet, **Back and Forth Transfer and Coherent Coupling in a Cold Rydberg Dipole Gas**, *Phys.Rev.Lett.* 95, 233002 (2005).
- [25] J.O.Day, E.Brekke, T.G.Walker, **Dynamics of low-density ultracold Rydberg gases**, *Phys.Rev.A*, 77, 052712 (2008).
- [26] M.Mack, J.Grimmel, F.Karlewski, L.Sárkány, H.Hattermann, J.Fortágh, **All-optical measurement of Rydberg-state lifetimes**, *Phys.Rev.A*, 92, 012517 (2015).
- [27] B.W.Shore, N.V.Vitanov, **Overdamping of coherently driven quantum systems**, *Contemporary Physics*, 47, 341 (2006).
- [28] L.Asteria, *De-excitation dynamics of cold Rydberg atoms*, Master Thesis (2016).
- [29] A.L.de Oliveira, M.W.Mancini, V.S.Bagnato, L.G.Marcassa, **Measurement of Rydberg-state lifetimes using cold trapped atoms**, *Phys.Rev.A*, 65, 031401(R) (2002).
- [30] T.Zhou, B.G.Richards, R.R.Jones, **Absence of collective decay in a cold Rydberg gas**, *Phys.Rev.A*, 93, 033407 (2016).
- [31] D.B.Branden, T.Juhasz, T.Mahlokozera, C.Vesa, R.O.Wilson, M.Zheng, A.Kortyna, D.A.Tate, **Radiative lifetime measurements of rubidium Rydberg states**, *J.Phys.B*, 43, 015002 (2009).
- [32] I.Beterov, private communication.
- [33] T.Wang, S.F.Yelin, R.Côté, E.E.Eyler, S.M.Farooqi, P.L.Gould, M.Koštrun, D.Tong, D.Vrinceanu, **Superradiance in ultracold Rydberg gases**, *Phys. Rev. A*, 75, 033802 (2007).

- [34] P.Schauß, M.Cheneau, M.Endres, T.Fukuhara, S.Hild, A.Omran, T.Pohl, C.Gross, S.Kuhr, I.Bloch, **Observation of spatially ordered structures in a two-dimensional Rydberg gas**, *Nature*, 491, 87 (2012)
- [35] M.Marcuzzi, E.Levi, W.Li, J.P.Garrahan, B.Olmos, I.Lesanovsky, **Non-equilibrium universality in the dynamics of dissipative cold atomic gases**, *New J.Phys*, ISSN 1367-2630 (In Press) (2015)
- [36] E.Fermi, **Sopra lo spostamento per pressione delle righe elevate delle serie spettrali**, *Nuovo Cimento*, 11, 157 (1934).
- [37] B.D.Esry, C.H.Greene, **Validity of the shape-independent approximation for Bose-Einstein condensates**, *Phys.Rev.A* 60,1451 (1999).
- [38] V.Bendkowsky, B.Butscher, J.Nipper, J.P.Shaffer, R.Löw, T.Pfau, **Observation of ultralong-range Rydberg molecules**, *Nature*, 458, 1005 (2009).
- [39] G.Quémener, P.S.Julienne, **Ultracold molecules under control!**, *Chem.Rev.*, 112, 4949 (2012).
- [40] S.D.Hogan, F.Merkt, **A new perspective on the binding power of an electron**, *Chem.Phys.Chem.* 10,2931 (2009).
- [41] <http://steck.us/alkalidata/rubidium87numbers.1.6.pdf>
- [42] T.Okoshi, K.Kikuchi, A.Nakayama, **Novel method for high resolution measurement of laser output spectrum**, *Electronics Lett.*, 16, 16, 630 (1980).
- [43] W.Demtröder, *Laser Spectroscopy Vol:2 Experimental Techniques*, Springer (2008).
- [44] C.Cohen-Tannoudji, D.Guéry-Odelin, *Advances in Atomic Physics-An Overview*, World Scientific (2011).